THESIS FOR THE DEGREE OF LICENTIATE OF ENGINEERING

Tellurium interaction with surfaces in the containment and sea-salt residue

FREDRIK ESPEGREN

Nuclear Chemistry
Department of Chemistry and Chemical Engineering

CHALMERS UNIVERSITY OF TECHNOLOGY

Gothenburg, Sweden 2018

Tellurium interaction with surfaces in the containment and sea-salt residue

© Fredrik Espegren, 2018

Licentiatuppsatser vid Institutionen för kemi och kemiteknik
Chalmers tekniska högskola
Nr 2018:09

Nuclear Chemistry
Department of Chemistry and Chemical Engineering
Chalmers University of Technology
Se – 412 96 Gothenburg
Sweden
Telephone +46(0)31-772 1000

Printed by Chalmers Reproservice
Gothenburg, Sweden 2018

Tellurium interaction with surfaces in the containment and sea-salt residue

Fredrik Espegren

Department of Chemistry and Chemical Engineering, Nuclear Chemistry and Industrial Materials Recycling, Chalmers University of Technology

Abstract

In the event of a nuclear accident, the release of radionuclides is always a concern. The extent of such releases is affected by several factors, for example type of atmosphere, temperature, and what structural materials are present during the accident. The release of tellurium is especially worrying due its volatility, reactivity, and decay product of iodine. Moreover, the radiological and chemical toxicity of tellurium will during an accident be considerably problematic, to the public and nature.

This work is divided into two experimental parts in order to determine: (1) the interaction between tellurium and metallic structural material found in the containment and (2) investigate the potential effect when using seawater as a coolant focusing on sea-salt residue. All experiments were performed at the relevant temperature (depending on the which part) under oxidizing and inert conditions and for the containment experiments humidity was also investigated. The structural material investigated were the metal surfaces aluminum, zinc, and copper with the aim of determining morphology, chemical speciation and if a reaction occurred between the metal surface and tellurium. For the investigation of seawater, determining if a chemical reaction(s) between tellurium and sodium chloride occurs and at what temperature.

Results from the containment experiments using a furnace showed signs of possible reaction between tellurium and the copper surface under inert humid conditions close to room temperature. Otherwise, tellurium deposition occurred on the metal surfaces with no observable chemical reaction and no strong attachment to the surface. The deposit formed on the surfaces and the observed chemical species under the different conditions, determined using different spectroscopy methods, were as follows: TeO_2 under oxidizing with (crystal structure paratellurite) and without humidity (crystal structures: paratellurite and orthorhombic), Te-metallic under inert conditions both with and without humidity, and finally Cu_7Te_4 was seen in the deposits on the copper surface under humid inert conditions.

For the seawater investigation, two methods where used thermogravimetric analysis and furnace experiments. The results from these methods showed that under inert conditions, no indication of interaction was seen. However, for oxidizing conditions an interaction for all samples was observed that prevented an otherwise seen mass increase of the tellurium reference. Through the furnace experiments, the appearance of the samples at increasing temperatures were studied and used to support the thermogravimetric analysis.

Keywords: tellurium, server nuclear accident, chemistry, containment, deposition, seawater

Contents

1 Introduction

A pressing concern within the European Union (EU) today is energy production and the supply for its production. This was evident during the winters of 2006 and 2009 when the gas supplies to the eastern part of the EU were cut off. Such a scenario and others have shown the need for the diversification of energy sources, a higher level of stability and access to abundant supply. These are among the goals included in the "*European Energy Security Strategy*" from 2014 [1]. Part of the energy needed comes from the use of electricity and a proposed solution for electricity production is nuclear power. This is supported by the strategy, as it states that nuclear power is capable of providing a "reliable base-load electricity of emission free supply" [1]. Moreover, it is also stated that the EU maintains a prominent position when it comes to all aspects of nuclear fuel production [1].

For nuclear power to be a viable source of energy from a public standpoint, safety is essential. This is emphasized in the statement, as it states that: *"The EU should remain the pioneer and architect for nuclear safety at international level"* [1]. For this to remain viable, investments and research in nuclear safety of both old and new reactor concepts are needed.

In 2011 the most recent known nuclear power accident known to the public occurred in the Fukushima prefecture, Japan. The consequences of this accident were not only felt on a local level but also globally at most nuclear power plant sites. One example of this was the almost immediate call after the accident for extensive stress tests to be carried out within the EU of all nuclear power plants to determine their readiness for an unexpected extreme event (e.g. earthquakes, tsunami).

Still, should an accident occur (similar to the severity of Fukushima), knowledge of the potential radiological releases would be important. Therefore, it is necessary to gain a better knowledge of the mechanism behind the releases, transportation and chemical processes of the many radionuclides that could be released to the environment during an accident and thus expose the public to potential harmful radioactivity. Moreover, should emergency actions have to be taken during a nuclear accident the effect of these will also have to be considered. Such actions were taken during the Fukushima accident, when loss of normal cooling water resulted in the need to use seawater for cooling. Considering these topics, research related to them could enable the design of mitigating measures against releases and reducing or restricting the consequences of a nuclear accident.

In recent years, the main focus of nuclear accident management has been on the modeling of nuclear accident scenarios. In these models, a wide range of phenomena within e.g. the fields of physics and chemistry are being considered. However, the discovery and evaluation of the relevance of these phenomena and their impact during nuclear accidents require extensive experimental data. Thus,

it is imperative that the experimental work is carried out alongside the modeling effort to explore and understand these phenomena. There are several ways in which such experimental data can be acquired. One way is through massive, time-consuming and nation spanning experimental projects such as VERCORS and PHÉBUS [2, 3, 4, 5, 6, 7], whereas many phenomena as desired can be explored at the same time and thus more closely mimic an actual accident. An alternative is bench-scale works [8, 9, 10, 11] dedicated to a specific topic (e.g. iodine, ruthenium chemistry), where the aim is to explore and understand one or very few phenomena. Observing the data from both the larger and smaller projects, a lack of tellurium specific chemistry in the containment and elsewhere can be observed. Therefore, the focus of this work is aimed at better understanding the behavior of tellurium in the containment as well as some ways in which tellurium volatility could be enhanced.

1.1 Objectives

The experimental work described here is divided into two parts. The first part focuses on how tellurium is affected and behaves in the containment as it is exposed to the different surfaces found in the containment. The second part considers the action taken during the Fukushima accident, where sea-water was used to maintain the cooling capability of the nuclear reactors. As sea-water contains salt, there is a likelihood that the salt could enhance the tellurium source term through formation of more volatile chemical species of tellurium.

2 Background and theory

2.1 Nuclear accidents

In order to determine the severity of an incident relating to radiation sources, the International Atomic Energy Agency in collaboration with the Nuclear Energy Agency of the Organization for Economic Co-operation and Development created in 1990 the International Nuclear and Radiological Event Scale (INES). It evaluates all incidents, at any facility with activities relating to the use of radiation sources. The scale considers not only events where releases of radioactive material have occurred to the environment or when workers and the public have been exposed to radiation, but also incidents without consequences where the safety features put in place have failed [12].

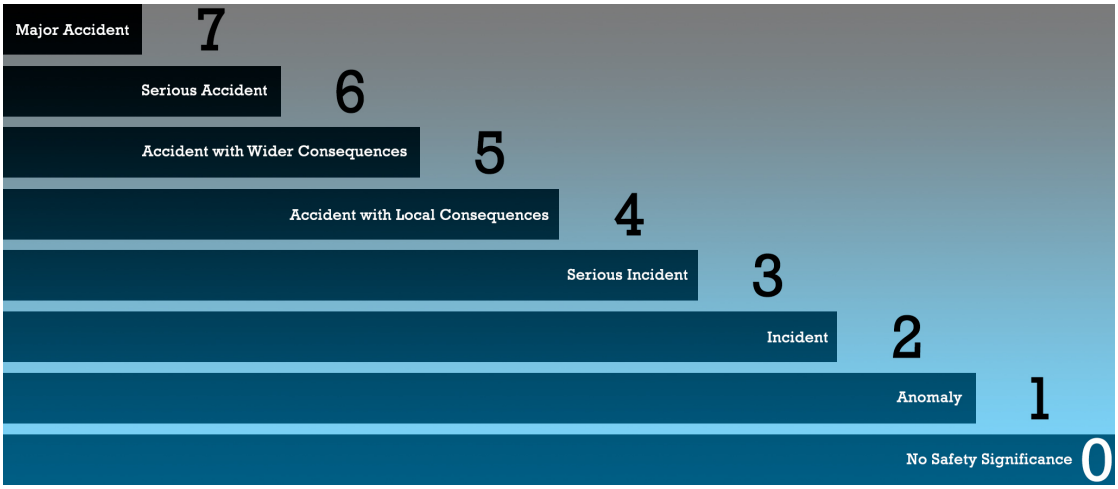

Figure 1. A rendition of the international nuclear and radiological event scale, remade based on [12].

In total, there are 7 levels on the scale, where each step up indicates a severity increase of magnitude 10. However, a level designated as 0 exists as well to include all incidents without a significant safety concern [12]. These levels are exemplified in Figure 1.

Since the beginning of civilian nuclear power plant operations, two accidents have reached a classification of level 7; the infamous Chernobyl accident [13] in 1986 and the Fukushima-Daiichi accident [14] in 2011. During these, and other accidents, one of the most worrying aspects has been the release of a radionuclide to the environment, considering that the consequence of these releases can be unwanted exposure to the general public and render landmasses unusable.

In the context of nuclear accidents, the terminology "*Source Term*" is used.

This can be defined (as there is no generally accepted definition) as: "*the quantity, time, history, chemical and physical form of radionuclides released to the environment, or present in the containment atmosphere, during the course of a severe accident*" [15].

2.1.1 Nuclear accident scenarios

From the point of the radionuclides, the progression of a nuclear accident leading up to a core meltdown can be divided into several phases. These are; a minor radionuclide release phase and two main radionuclide release phases. The two latter phases are referred to as the in-vessel and ex-vessel phases. Moreover, it is possible to further subdivide these into an early and late stage phase.

The minor release phase (and the start of source term evaluation) is when radionuclides are released from the core and occurs when the cladding surrounding the fuel fails, as prior to this the gap has been filled with radionuclides that have been released to the gap during normal operations. When the failure occurs, a pathway for the most volatile radionuclides (e.g. noble gases, iodine) appears and releases can start. This release phase constitutes a small percentage of the total fuel content of these radionuclides and last roughly 30 minutes, ending when the temperatures have reached levels; at which the main bulk of radionuclides will no longer remain in the fuel [15].

As the temperature increases and finally reaches levels where the core starts to lose structural integrity, the phase is known as the early in-vessel phase begins. During this phase, the most volatile radionuclides (e.g. noble gases, iodine) start to escape in higher amounts compared to the previous phase, alongside some of the lesser volatile radionuclides. As this phase progresses the core eventually reaches the bottom of the reactor vessel and the early in-vessel phase ends when the corium (molten core debris) finally breaches the bottom of the reactor vessel. The early in-vessel phase is estimated to take more than 10 min, but the duration of this process is dependent on the type of reactor and accident scenario [15].

After the molten corium has fallen down to the concrete floor beneath the reactor vessel, the next two phases begin; ex-vessel and late in-vessel. Outside the reactor vessel, the ex-vessel phase, the molten corium will have reached the concrete and reactions between them occur, thus increasing the amount of radionuclides being released. Only first when the corium has reached sufficiently low temperatures does the ex-vessel phase end (few hours). Inside the reactor vessel, the late in-vessel phase, potential re-volatilization of already deposited radionuclide can happen as well as further releases from the fuel. This phase lasts for around 10 hours [15].

To eventually reach the environment, two paths are possible. Either the containment has failed, resulting in the by-passing of it by the radionuclide (e.g. pres-

sure water reactor (PWR) steam generator tube ruptures), or the containment remains intact and the radionuclides enter the containment. Inside the containment, safety features can be used to mitigate the actual release of radionuclides to the environment. Such features are e.g. containment spray (removing particles from the air), pH control of sump water (trapping iodine) or filtering of the venting air (removing aerosols of radionuclides) [15]. For such counter measurements to be at all conceived and implemented, knowledge (chemical and physical) of the radionuclides in the containment is necessary.

2.2 Fission products

The radionuclides that are released during an accident scenario, e.g. as mentioned in the previous chapter, originate mainly from the fission of the fuel content. In the current nuclear fleet, the most common fuel type is the cylindrically shaped uranium dioxide with enriched amounts of ^{235}U. Alternatively, the mixed oxide (MOX) fuel type is also used. In this fuel, Pu has been added to the fuel alongside the ^{235}U by breeding or reprocessing from spent uranium fuel [16].

The actual production of the energy needed to produce the electricity comes from fission of the uranium and the plutonium (the fissile material). This is achieved by splitting (e.g. fission) of the fissile atoms with neutrons and consequently the production of high kinetic energy fission fragments (fission products) and more neutrons. The fission products, rapidly dissipate their energy (average energy released from a fission is $\sim$200 MeV) to the surrounding media [17]. The surrounding media, mainly consisting of the coolant (e.g. water, heavy-water), is then heated. Depending on the reactor type, the water (or steam) is transported away to be used in steam turbines (directly or indirectly, through heat exchangers) for electricity production.

Each fission product has a different yield from the fission of different fissile material. In Figure 2 the fission yield of ^{235}U, ^{239}Pu and ^{241}Pu from thermal neutrons can be seen, reproduced from data produced by the Japan Atomic Energy Agency [18].

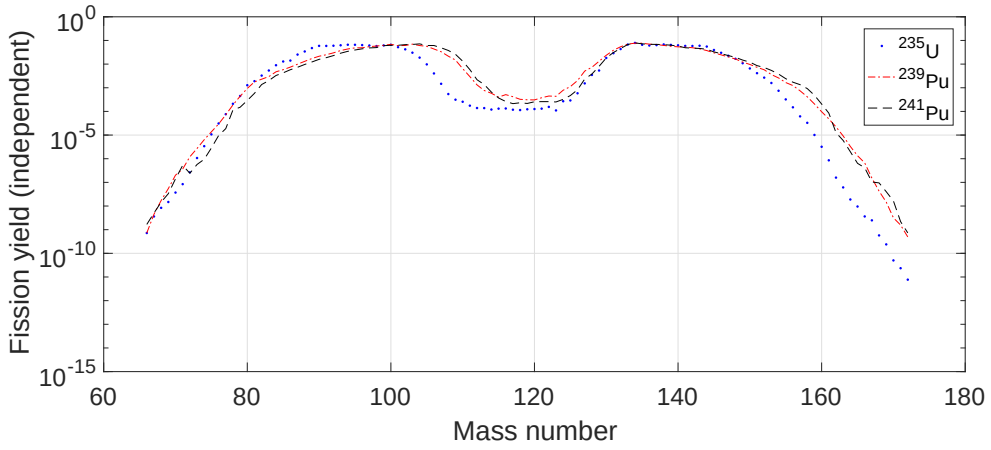

Figure 2. Fission yield (from thermal neutrons) for the fission fragments sorted after the mass number, as produced from the fissile materials ^{235}U (blue), ^{239}Pu (red) and ^{241}Pu (black) [18].

To identify which mass numbers, and thus which fission products, are of importance for nuclear accident consideration, the fission products can be classified according to their volatility. A summary of this can be seen in Table 1 [15].

Table 1. A possible classification of the fission products (FP) based on the outcome of the PHEBUS experiments [15].

Classification	Fission product/gas
Volatile Gas and FP	Kr, Xe and I, Cs, Br, Rb, Te, Sb
Semi-volatile FP	Mo, Rh, Ba, Pd, Tc
Low-volatile FP	Sr, Y, Nb, Ru, La, Ce, Eu
Non-volatile FP	Zr, Nd, Pr

The degree of volatility of the fission products in Table 1 are based on the outcome of the PHEBUS experiments. However, many parameters can change the volatility of these fission products. Some of these parameters might not necessarily have been explored during these experiments. A summary of some of the main physical parameters that affect the fission products are temperature, oxidizing/reducing conditions, interaction with cladding/structural material, burnup, fuel type and state of the fuel [15].

Since different fission products are differently affected by these parameters, it is important to investigate each fission product separately to better understand their behavior during a severe nuclear accident. Thus, this thesis focuses on the source term of tellurium.

2.2.1 Tellurium; radiological point of view for nuclear accidents

The main isotopes of tellurium produced in a reactor during normal operations are ^{131}Te, ^{132}Te, ^{133m}Te and ^{134}Te. These isotopes constitute roughly 60% of the tellurium content [19]. The corresponding mass numbers of these isotopes belongs to the upper part of the yield curve, as shown in Figure 2. Moreover, the specific fission yield of the corresponding tellurium isotopes mass number can be seen in Table 2.

Table 2. The fission yield from ^{235}U and ^{239}Pu. In addition, the relevant tellurium isotope mass number, their decay modes, half-life ($t_{1/2}$) and parent (P) to daughter (D) product are included [20]. "A" is the mass number, "m" represents metastable, and "DM" represents decay mode.

A	^{235}U [%]	^{239}Pu [%]	DM 1 ($t_{1/2}$)	DM 2 ($t_{1/2}$)	P/D
131	2.878	3.724	m, β^- (33.25 h)	β^- (25 m)	^{131}Te/^{131}I
132	4.296	5.274	β^- (76.3 h)		^{132}Te/^{132}I
133	6.6	6.99	m, β^- (55.4 m)	β^- (12.5 m)	^{133}Te/^{133}I
134	7.79	6.87	β^- (41.8 m)		^{134}Te/^{134}I

The half-life of the tellurium isotopes is generally short, as seen in Figure 2. Furthermore, the decay product of the isotopes are all iodine, which is another reason for the importance of tellurium source term evaluation, as the tellurium releases will contribute to iodine releases [19].

The inventory of a 900 MWe PWR for the different fission products at end-of-life have been calculated elsewhere using the DARWIN-PEPIN code [15]. For the calculation the core was initially loaded with $72.5{\cdot}10^3$ kg uranium divided over four quarters, which had reached individual burnups of 10.5, 21, 31.5 and 42 GWd/t at the end. The calculated value for tellurium at shutdown was 26.2 kg, which can be compared to other volatilize fission products in Table 1, e.g. iodine 12.7 kg and cesium 161 kg. In comparison to iodine, the core content of tellurium is significant. Should this be released, the tellurium would contribute considerably to radioactive releases during a nuclear accident.

2.2.2 Tellurium; chemical point of view for nuclear accidents

The chemical form of tellurium in the fuel is considerably complex. For example, it can form oxides and several metallic phases with e.g. uranium, palladium and tin [21]. Studies have indicated that Cs_2Te [22], TeO_2 [22], TeI_x [23] PdTe [24] and BaTe [24] will exist in the fuel during normal operations. Moreover, during operations there would be minor amounts of tellurium released to the fuel-cladding gap. Tellurium species found in the gap are suggested to be Cs_2Te [22, 24] and

Te/Te_2 [24]. However, it is expected that tellurium would react with the Zircaloy cladding and thus not remain in any significant amounts in the gap [25, 26, 27, 28].

What chemical species of tellurium that would be expected to leave the core during an accident, will depend strongly on the conditions, e.g. oxidizing or reducing. As an example, it was seen during the VERCORS experiments [5] that significant releases of tellurium occurred first when the cladding had oxidized. This indicates that oxidizing conditions are important for tellurium releases from the core.

The explanation of the need for oxidizing conditions was found to be that tellurium is being retained in the Zircaloy cladding, through the formation of zirconium telluride. Thus, tellurium was only released when the zirconium had sufficiently oxidized. A potential way for oxidation of the zirconium present in the cladding can occur with steam, as Equation 1 shows [29].

$$Zr + 2H_2O \rightarrow ZrO_2 + 2H_2. \tag{1}$$

The resulting products for tellurium reacting with the Zircaloy in the cladding, are $Zr_{1+x}Te_2$ and Zr_5Te_4 [25].

When the cladding has oxidized completely, an initial surge of tellurium release occurs that would eventually slow down to levels closer to other volatile fission product releases. The chemical species leaving will be either metallic tellurium or SnTe. The latter is possible as tin is present and segregates inside the Zircaloy cladding. Thus, it is possible for tellurium and the tin to react when the cladding is fully oxidized. However, as already stated, the prevailing conditions will dictate the releases of tellurium and this is also true for SnTe. It was shown by calculation and experimental data by Boear and Cordfunke [26], that at high oxygen pressure (i.e. $H_2O/H_2 = 100/1$) tin reacts with oxygen and forms tin oxides. Moreover, it was also pointed out that the SnTe would dissociated into SnO_2 and Te-metallic [25, 26, 27]. The latter would also have the potentiality for oxidation, where TeO_2 (low and high temperatures) and TeO (high temperatures) would form [19].

The next stage for the tellurium releases is the primary circuit. The tellurium speciation in this stage will greatly depend on the preceding steps. The initial species may be e.g. SnTe, Te/Te_2, TeO and Cs_2Te. However, there is a potential for the tellurium species to change inside the primary circuit as well, due to the conditions and obstacles found therein.

Therefore, new tellurium chemical species (a "permanent" or transient change) could emerge inside the primary circuit. Starting with tellurium interacting with steam at high temperatures, e.g. $TeO(OH)_2$ (suggested under oxidizing conditions, the possible reactions are 2 [19, 30, 31] and 3 [32]) and H_2Te (reducing or neutral

conditions) [22, 19].

$$TeO_2(g) + H_2O(g) \rightleftarrows TeO(OH)_2(g) \tag{2}$$

$$TeO_2(g) + H_2O(g) \rightleftarrows TeO(OH)_2(g) + \frac{1}{2}O_2(g) \tag{3}$$

Moreover, by oxidation of tellurium forming TeO [19], by e.g. Equation 4 [31] and TeO_2 [19, 33] (formed by combustion in air [31], as exemplified by Equation 5).

$$Te + \frac{1}{2}O_2 \rightleftarrows TeO \tag{4}$$

$$Te + O_2(g) \rightleftarrows TeO_2 \tag{5}$$

There is also a potential for tellurium to react with different types of reactor materials. For example, it has been seen that tellurium reacts with 304 stainless steel, forming $Fe_{2.25}Te_2$, or if an oxide layer is present on the stainless steel surface $FeTe_2$. Another reactor material that can react with tellurium is the Inconel 600 alloy, where $Ni_{2.86}Te_2$ or $NiTe_2$ can form. The latter is formed if the Inconel 600 is covered by an oxide layer [34]. Finally, due to changes of temperature affecting different tellurium species stability H_2Te for example is present only above 1400 K,whereas Cs_2Te is not stable above 1400-1600 K [22].

From the primary circuit, two potential pathways are possible. Either tellurium will by-pass the containment and be directly emitted to the environment; e.g. by PWR steam generator tube ruptures[1] or interfacing systems loss of cooling accidents[2]; or tellurium will enter the containment, thus being subjected to the conditions and structural material found there. In this work, the latter of these scenarios will be the continued focus.

Entering the containment, the chemical species (e.g. Te/Te_2, Cs_2Te and SnTe) will again be exposed to new conditions, and surfaces. These can be: aerosols made up of structural and control rod material from the core, other fission products, air, liquid water, organic material (e.g. paint), metal and concrete surfaces [35]. The information on the tellurium behavior and chemical speciation in the containment is limited. However, it is expected that most of the tellurium species would condense on the surface in the containment and enter the sump water (directly or be washed into it). Moreover, it is also a possibility that tellurium will react (especially when condensed steam is present) with metals and painted surfaces to form metal and organic telluride, which can be more volatile than other non-organic species of tellurium [22, 35].

[1] As a consequent of the steam generator safety valves failing, the radionuclides enter the environment from the secondary side of the steam generator.

[2] A system outside the containment is breached, e.g. the auxiliary building.

Lately, a new concern has become a more pressing consideration for nuclear accidents; the potential for revaporization or physical resuspension of fission products. The relevance of revaporization for tellurium in the primary circuit was shown to be considerable [36]. However, revaporization might also be a concern in the containment. The conditions in the latter will not be as erosive as in the primary circuit, but conditions might be sufficient to induce revolatilization.

For the first part of the work, surfaces found throughout the containment are of interest. At the Swedish BWR (boiling water reactor) nuclear power plants, the main surfaces found in the containment will be epoxy painted concrete (not within the scope of this work), estimated to be around 2000-3000 m^2 [11], construction material made from aluminum, with a surface estimate of 11930 m^2 [11] and zinc used to galvanize metal surfaces, corresponding to total zinc surface of 6300 m^2 [11]. Moreover, it is also possible for copper aerosols to enter the containment. These aerosols would originate from cables and are expected to cover (assuming an average diameter of 10 µm) a surface in the containment corresponding to 1350 m^2 [11, 37].

2.3 Tellurium and sea-salt

To avoid overheating and melting of the core during a nuclear accident, maintaining adequate cooling is necessary. Therefore, a cooling media is always needed. Should the engineered system fail, other nonconventional sources may be needed. For light water reactors located on the coast, a potential non-conventional source could be seawater. However, using this introduces new sources of uncertainties, i.e. the content of the seawater. In seawater the most abundant elements are Cl^- (16.58 $g/kg_{seawater}$ [38]) and Na^+ (9.03 $g/kg_{seawater}$ [38]). Thus, these two elements have the greatest potential for interaction with the fission products.

There exists a range of possibilities for where this interaction could take place. One scenario, the one considered in this work, is that sodium chloride has deposited on surfaces inside the containment, or possibly on the fuel-assembly itself. This scenario could happen through evaporation of seawater as a consequence of insufficient cooling. If this scenario was to occur, new surfaces could emerge from under the seawater, with salt residue on them. Thus, these emerged surfaces could enable reaction between sodium chloride (as the salt residue) and any fission product that can reach these surfaces. Therefore, it would be possible, depending on the temperature, that a reaction could occur between two solids, two liquids, two gases, or at any of the phase boundaries (considering the difference in melting point and boiling point of the sodium chloride and the different fission products) of the sodium chloride and fission products.

The effect of seawater use as a coolant on the different fission products source term has not been investigated to any greater extent in the literature. Therefore,

it is unclear how the use of seawater would affect the releases of fission products. However, it has been observed [39] from the Fukushima accident that the released activity of ^{95}Nb did not follow the expected physical decay, predicted from modelling. Instead the activity increased over time, indicating not only a point release but rather a continuous one. A potential explanation for this was suggested to be halide formation of niobium, considering the difference in the boiling points of its halide (e.g. $NbCl_5$ has a boiling point of 520 K [40]) compared to the metallic state (5014 K [40]) of niobium (and/or potentially its parent ^{95}Zr) can be considerable [39]. Thus, the use of seawater could have enabled the formation of halides due to the chloride content of seawater.

Therefore, it is possible that interaction between sodium chloride and fission products other than niobium is also possible. A potential candidate for this interaction is tellurium, as it is chemically considered reactive [19]. Moreover, observing the melting points and boiling points of the tellurium metal, oxides, and chlorides in Table 3, the formation of tellurium chlorides would increase the source term of tellurium (as the boiling point would decrease).

Table 3. Tellurium oxide and chloride species and some their properties. TeO has not been included, as it has not been shown to exists in solid state [31]. Solubility in water. "MP" represents melting point and "BP" represents boiling point.* depended on the crystal structure, e.g. yellow if orthorhombic structure.

Species	MP (K) [40]	BP (K) [40]	Appearance	Solubility [41]
Te	723	1261	Grey-white [40]	Insoluble
TeO_2	1006	1518	Colorless/yellow* [42]	Insoluble
$TeCl_2$	481	601	Black [42]	Decomposes
$TeCl_4$	497	660	Pale-yellow [42]	Decomposes

Moreover, the chlorides of tellurium decompose in water. Therefore, a reaction between sodium chloride and tellurium, where the tellurium chloride remains after the reaction, would most likely occur on an exposed surface.

An alternative to the formation of tellurium chlorides could be tellurium oxychloride, based on the analogy of selenium. However, the existence of such a species has never been verified [43]. Still, it is possible that a tellurium oxychloride exits only as a transient species, requiring specific conditions

3 Experimental

3.1 Containment experiments

The containment experiments were carried out using a tubular furnace (ETF 30-50-18-S, Entech). Inside the furnace, a 130 cm high purity alumina tube (Al_2O_3, 99.7 %, Degussit AL23, Aliaxis) was placed. To enable the connection of gas lines to the tube, connectors (stainless steel, custom made) were added at both ends. Connected prior to the inlet connector was a gas trap filled with MQ water (Millipore, 18 MΩ) through which the gas could bubble prior to entering the tube(for the conditions requiring increased humidity). At the other end, the outlet connection was designed with an internal shape of a cone to promote smoother transition for the exiting gas flow. From the outlet, the exiting gas was transported to a water-filled gas trap (Millipore, 18 MΩ). The latter was to prevent tellurium escaping the system as well as to act as a water lock. In Figure 3 a schematic overview of the setup used can be seen.

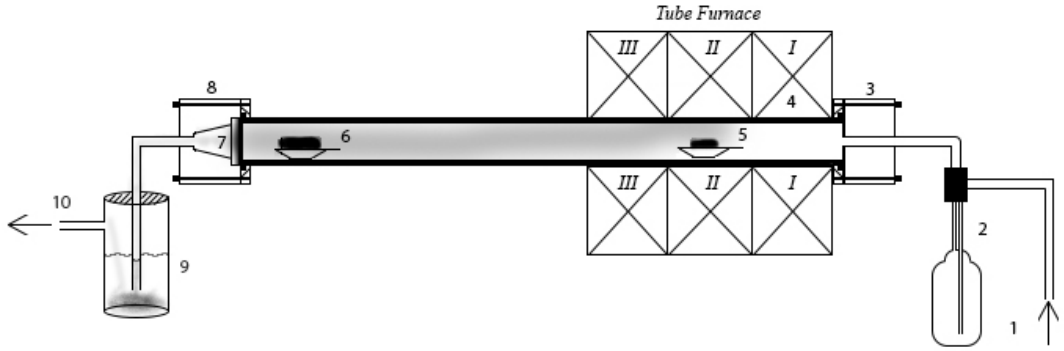

Figure 3. The experimental schematics for part one: (1) gas flow inlet, (2) the water source, consisting of a water bottle, (3) cylindrical formed inlet connector made from stainless steel, (4) tube made from Al_2O_3 with a length of 130 cm, (5) the source for the material to be volatilized,(6) the metallic coupon, (7) cone formed outlet, (8) connector made from stainless steel, (9) one or several cold traps used to prevent escaping particles and (10) gas flow outlet. The furnace is divided into three heat zones: in Heat Zone I the gas flow is heated to the programmed temperature, in Heat Zone II the gas flow maintains at least the programmed temperature and Heat Zone III the gas flow starts to cool down.

The investigated surfaces were acquired as either a rod or a sheet, thus requiring these to be cut into more manageable sizes. The aluminum rod (diameter: 19 mm, 99.5 %, Alfa Aesar) and zinc rod (diameter: 13 mm, 99.5 %, Alfa Aesar), were cut into discs with a thickness of 3 mm. The copper sheet (thickness 3 mm, 99.5 %, Sigma Aldrich), was made into square coupons of 10x10 mm size. A representative image of each coupon can be seen in Figure 4.

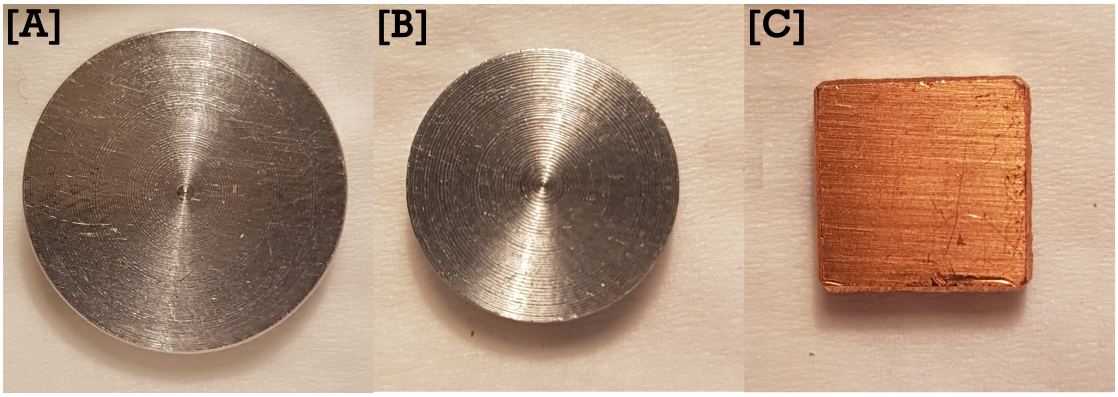

Figure 4. The general appearance of the coupon surface made from (A) aluminum, (B) zinc and (C) copper before being used in an experiment.

The tellurium (99.8%, Sigma Aldrich) used during each experiment, was evenly spread out inside a crucible (boat, porcelain 85x13x8 mm, VWR), the amount used was 1-2 g (1 g for inert[3] and 2 g for oxidizing). The crucible with tellurium was then placed in the middle of the furnace, inside the tube. The coupon made from one of the metals was positioned on a crucible, at the outlet. At this location, the temperature was kept at a maximum of 339 ± 1.5 K[4]. The temperature was chosen to be as close to what is expected in the containment.

The transport of the tellurium to the coupon was achieved by a flow (1.5 l/min) consisting of the desired atmosphere, with and without increased humidity (see Table 4 for the difference of humidity). The atmospheres used corresponded to oxidizing (compressed air, Porter gas regulator) and inert (Ag, 99.999%, Air liquid, Aalborg gas regulator) conditions. For both atmospheres, the flow was maintained throughout the whole experimental run. Increasing the humidity of the gas flow was achieved by bubbling the gas through a gas trap filled with MQ-water to a hight of 8 cm, which corresponded to a total volume of 500 ml.

[3]The amount used during inert conditions had to be lowered as a back-flow of tellurium was observed.

[4]Based on an internal furnace temperature of 1478 ± 9 K yielded a value of 339± 1.5 at the outlet

Table 4. The relative humidity (RH) and absolute humidity (AH) of the different gas flow used during the containment experiments. Measured using a Fisherbrand™Traceable™Humidity Meter and was certified when purchased with an expanded measurement uncertainty of ±0.090 at 298 K. The values seen is the average of the minimum and maximum value after 10 minutes of measuring, as it was not possible to continuously record. The measurement was carried out at the outlet, without a connector attached.

Type	Humid (Y/N)	Temperature of furnace [°C]	RH [%]	AH [g/m^3]
Air	N	1000	<1	<1
Air	Y	1000	70	18
Argon	N	1000	<1	<1
Argon	Y	1000	76	19

All experimental runs were heated (10 K/min) from ambient temperature to isothermal temperature (1273 K[5]). The isothermal temperature was maintained for one hour and following this, the system was cooled (no heat control) to room temperature. The coupon was then removed from the system and post-analyzed.

3.1.1 Characterization of the deposition on the coupon surfaces

Scanning election microscopy (SEM) of the type FEI Quanta 200 environmental SEM, was used determine if a chemical reaction occurred between the coupon surface and the tellurium. Moreover, when no reaction was observed and only deposition occurred, the morphology and content of the deposition was of interest. The analyses were carried out in high vacuum and with a voltage ranging from 10-15 kV. No specific magnification was used, instead the magnification resulting in the clearest micrographs was chosen individually for each sample.

X-ray diffraction spectroscopy (XRD) was used for chemical speciation of the deposition on the coupon. Siemens Diffraktometer D5000 x-ray diffraction spectroscopy using CuKα characteristic radiation wavelength. The sample holder was set to rotate 360°/min and the detector measuring angle was 10°-90° (2θ). The obtained output data was compared to PDF-4+ 2018 diffraction data of crystals and powders.

As the deposition was made on a flat surface, the glancing angle approach was used [44]. This means that the incoming angle of the x-ray beam is fixed at a specific angle. The selected angle was based on the observations during the analysis. Thus, when the surface of the coupon was aligned with the top of the

[5]Chosen, based on the boiling point of tellurium

sample holder, an X-ray beam angle of 5°resulted in the highest intensity of the output signal from the depositions.

X-ray photoelectron spectroscopy (XPS) was performed using a PHI 5000 VersaProbe III scanning XPS microprobe. This technique was used when the XRD analysis did not yield a clear enough spectrum with possible peaks for chemical characterization. However, the XPS requires a high vacuum to operate and therefore the surface had to be removed from the coupon by carbon tape (carbon adhesive discs) prior to analysis. Therefore, the exposed surface is the one being analyzed.

When XPS is used the sample is bombarded with an X-ray beam (source: Al, 1486.6eV), which ionizes the electrons of the surface atoms. Consequently, photoelectrons are emitted and detected. These form a spectrum containing the photoelectrons kinetic energy, with intensity maximum. These intensity maximums are characteristics for an element, as they correlate to the binding energies of the photoelectrons, meaning that they can be used for elemental identification. Moreover, chemical speciation can also be performed, because when an element is part of a molecule this will result in a shift of the intensities. However, depending on the molecule, the spectrum may be complex, where an intensity maximum may contain several possibilities for the elemental identification [45].

When used, two measurements were performed for each analysis. First, an overview scan (0-1100 eV) using 280 eV pass energy, 44.5°take-off angle and using a stepping of 1 eV/step was performed to determine the binding energy ranges for which a focus scan was needed. For the focused scan the following parameters were used: 55 eV for the passing energy, 44.5°take-off angle and a stepping of 0.05 eV/step. The latter was used to gain a higher resolution of selected regions, covering C 1s, O 1s, Te 3d photoelectron intensity maxima.

3.2 Tellurium interaction with sea-salt

These experiments were performed to determine the potential effect that sodium chloride could have on tellurium. Therefore, two experimental procedures were designed and carried out.

The first experimental procedure was performed using a TGAQ500 thermogravimetric analysis (TGA) from TA instrument. This was done by using an alumina pan (TA instrument) containing the sample, which was cleaned prior to use with 1 M HNO_3 (70%, ACS reagent, Sigma Aldrich), MQ-water (Millipore, 18 MΩ) and dried in a heating cabinet overnight.

The samples used consisted of tellurium (99.8%, 200 mesh, Sigma Aldrich) and sodium chloride (99.5%, Acros Organics) of different ratios, where the latter

had been ground down using a mortar and pestle prior to mixing with the aim of creating a more homogenous mixture. In total, three samples with different mixing ratios were investigated: 4:1 (S1), 1:1 (S2) and 1:4 (S3) of tellurium and sodium chloride. Alongside these, two references consisting of either only tellurium (Ref1) or only sodium chloride (Ref2) were made. Three triplicates were made for each sample and reference, and these were added (8-10 mg) to the pans and gently spread out by tapping the side of the pan.

Two atmospheric conditions were investigated; inert (nitrogen, 99.98%, in-house gas) and oxidizing (synthetic air, 79%/21% nitrogen/oxygen, AGA). The conditions were established by introducing a constant gas flow (90 ml/min) of the desired atmosphere, which also transported away the volatilized material. Concurrently with this flow, another flow was used to support[6] the pan (10 ml/min, always nitrogen). Both the flow rates were monitored by the TGA-equipment.

The heating procedure of the TGA was programmed to cover a maximal temperature range. However, to avoid unnecessary complication of the TGA a safety margin from the maximum temperature for the TGA of 100 K was ensured. The experiment was started from ambient temperature and heated (5 K/min) to the isothermal temperature (1137 K). This temperature was maintained (20 min) and afterward the system was allowed to cool (aim: 10 K/min) until room. In between each experiment, cleaning was performed to remove residue deposited inside all piping extending from the furnace part of the TGA. This was followed by a run with an empty pan, under inert conditions using the same settings a previously described. During the heating, the mass is recorded with one second intervals. The temperatures were monitored by the TGA-equipment itself, without any external verifications.

In addition to the TGA experiment, a second experimental procedure was used. This procedure used same the tubular furnace as the one used during the containment experiment, with the system setup similar to that described in the previous chapter. However, the setup was slightly altered and the new schematics can be seen in Figure 5.

[6]This gas flow comes down onto the sample pan.

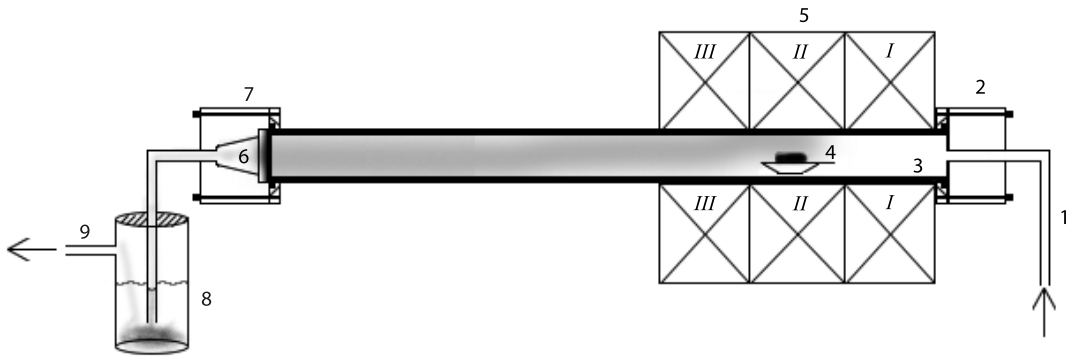

Figure 5. The experimental setup used: (1) gas flow inlet, (2) cylindrical formed inlet connector made from stainless steel, (3) ceramic tube of length 130 cm, (4) the mixture of compounds, (5) tubular furnace (6) a potential location to place a filter at the end of the tube, (7) cone formed outlet connector made from stainless steel, (8) cold trap used to prevent particles escaping and (9) gas flow outlet. The tubular furnace is divided into three heat zones: in Heat Zone I the gas flow is heated to the programmed temperature, in Heat Zone II the gas flow maintains at least the programmed temperature, and in Heat Zone III the gas flow starts to cool down

The goal of this part was to obtain a visual overview, when a mixture is heated to a selected temperature and then left to cool to room temperature. For this part only the 1:1-ratio of tellurium and sodium chloride was investigated.

The same supplier and quality of tellurium and sodium chloride (no grinding) as for the TGA analysis was used. However, the total amount of sample was increased to 2 g. The sample was evenly spread out in a crucible (boat, porcelain 85x13x8 mm, VWR), after which it was placed in the middle of the furnace inside the tube.

Only the oxidizing condition was investigated. The condition was established by a flow (1.5 l/min, Aalborg gas regulator), consisting of air (compressed air). To ensure an excess amount of oxygen, the flow was maintained throughout the whole experiment.

The experiment was heated (10 K/min) from ambient temperature to isothermal temperature (473 K and temperatures in the interval 573-1073K). This temperature was maintained for one hour and was followed by a cooling (programmed: 10 K/min[7]) of the system too until room temperature, with the maintained gas flow.

[7]In actuality this was much slower, as it was not possible to cool the system and so the system only stopped heating.

4 Results and discussion

4.1 Containment experiments

The results for the containment experiments can be seen under oxidizing conditions in Figure 6, inert conditions in Figure 7, when the humidity has been increased for oxidizing conditions in Figure 8, and the corresponding inert conditions in Figure 9. These figures show the coupons as found, directly after removing them from the system.

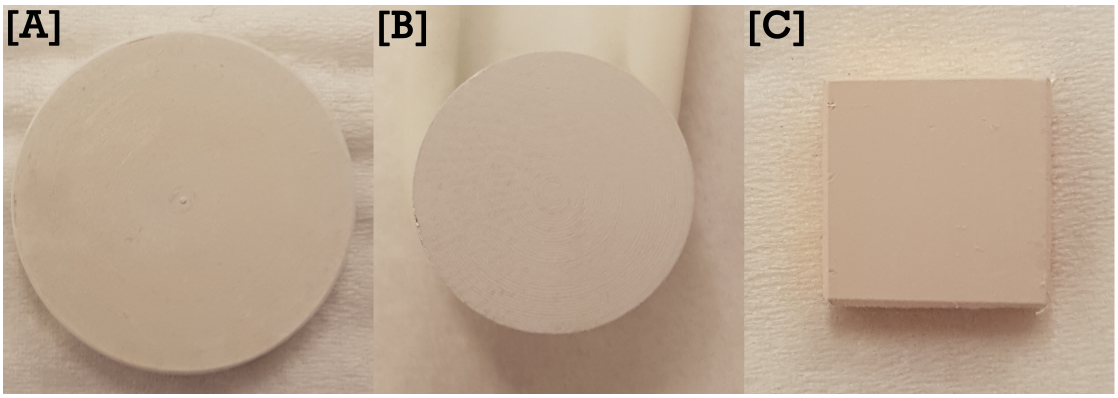

Figure 6. The resulting deposition on the coupons made from (A) aluminum, (B) zinc and (C) copper, from the experiment carried out in oxidizing condition.

For oxidizing conditions in Figure 6, the results for all three metals was a white deposition lacking any observable chemical interaction, as the deposition could be easily removed without any observable effects on the underlying surfaces.

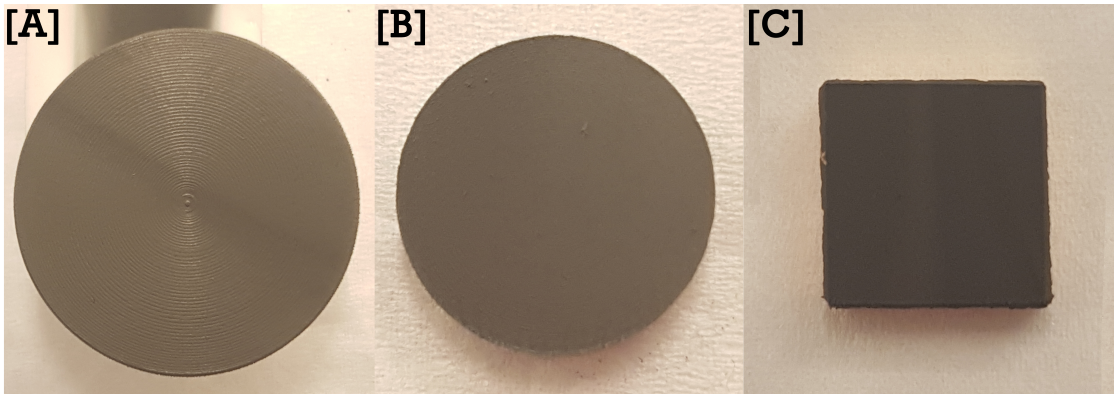

Figure 7. The resulting deposition on the coupons made from (A) aluminum, (B) zinc and (C) copper, from the experiment carried out in inert conditions.

In Figure 7 the experiment carried out under inert conditions shows that a black deposition was formed on all metal surfaces. Besides the color change, the results were very similar to the oxidizing conditions, as no chemical interaction was observed nor any visual changes to the underlying surface of all metals when the depositions were removed.

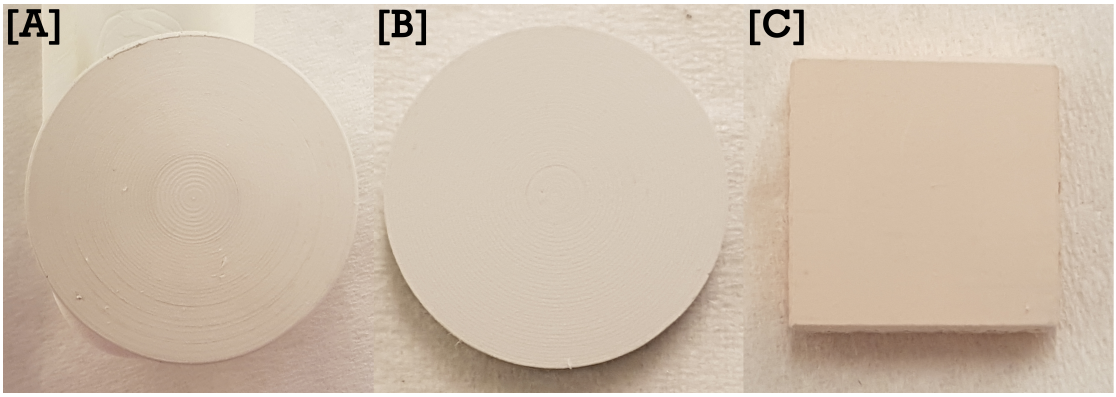

Figure 8. The resulting deposition on the coupons made from (A) aluminum, (B) zinc and (C) copper, from the experiment carried out in high humidity oxidizing conditions.

When the humidity was increased for the oxidizing conditions, the results can be seen in Figure 8. These were very similar to the outcome of the oxidizing conditions under less humidity, meaning that a white deposition lacking any interaction with the underlying surface for all metals was observed.

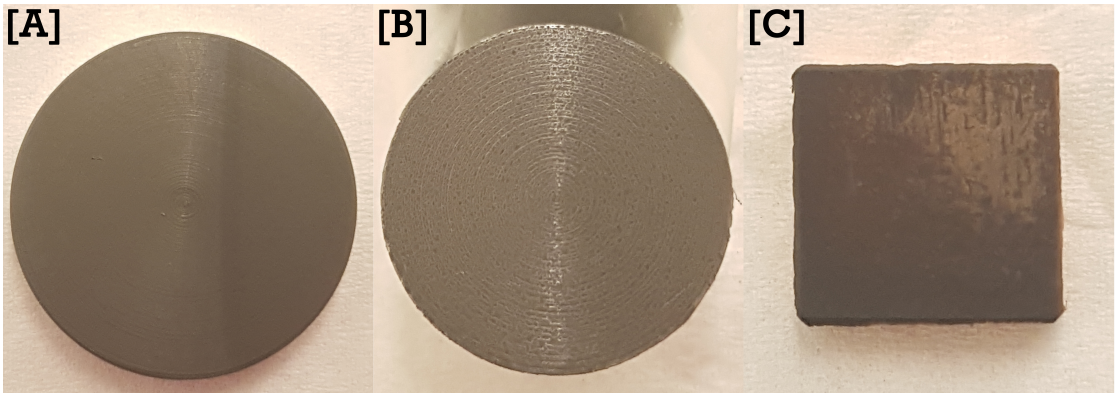

Figure 9. The resulting deposition on the coupons made from (A) aluminum, (B) zinc and (C) copper, from the experiment carried out in high humidity inert conditions.

For the experiment carried out under humid inert conditions, seen in Figure 9, the result for the aluminum coupon shows little difference from the less humid inert conditions experiment. However, the other two are somewhat different from

the inert experiments. A possible cause for the difference of the copper surface is described in section 4.1.2 and for the zinc no indication was found that the deposition was different.

4.1.1 Shape and morphology, SEM

To gain a better understanding of the surface deposition, micrographs were produced of the depositions made under oxidizing and inert conditions. These micrographs can be seen in Figure 10 the for aluminum surfaces, in Figure 11 for the zinc surfaces and in Figure 12 for the copper surfaces. However, no micrographs have been produced for the increased humidity cases.

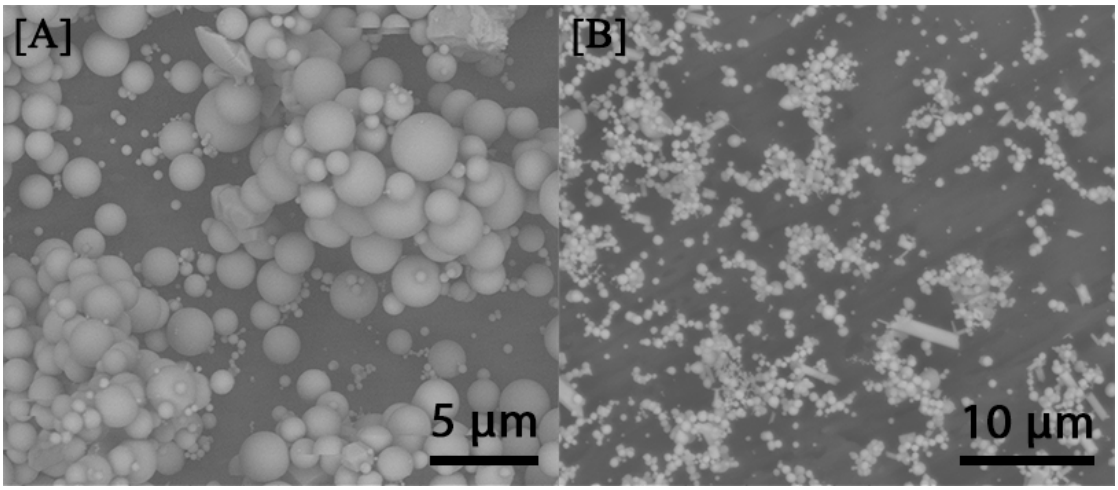

Figure 10. Micrographs of the depositions made on the aluminum coupon in (A) oxidizing less humid, and in (B) inert less humid conditions. For the micrograph for inert conditions (B), there was slight damage to the depositions prior to the analysis.

For the deposition made on the aluminum coupon under oxidizing conditions with no increased humidity (Figure 10 image A), what can be observed is mainly smooth spherical particles, alongside minor amounts of square and rectangular particles. When investigating inert conditions (image B) the main particle shapes were found to be smooth spheres, rectangular and spikes. No indication of a chemical interaction with the underlying surface was observed.

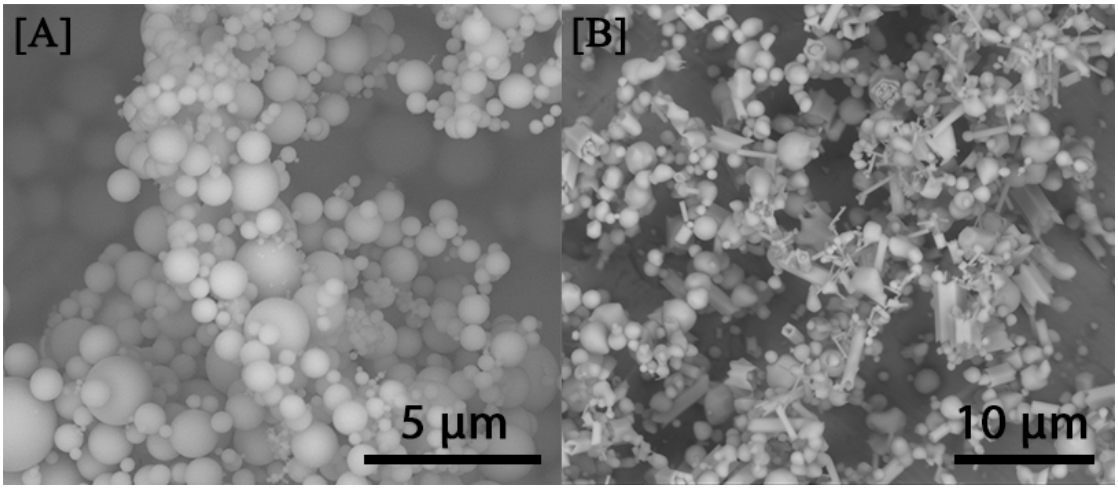

Figure 11. Micrographs of the depositions made on the zinc coupon in (A) oxidizing less humid, (B) inert less humid conditions.

The examination by SEM of the depositions made on the zinc coupon under oxidizing conditions (Figure 11 image A) showed mainly smooth particles with the occasional occurrence of rectangular/spike shaped particles. In the same figure (image B) the deposition produced under inert conditions on the zinc surface can be seen. In this deposition three shapes were observable, smooth spheres, rectangular and spike shaped particles. No chemical interaction with the underlying surface can be seen in either micrographs.

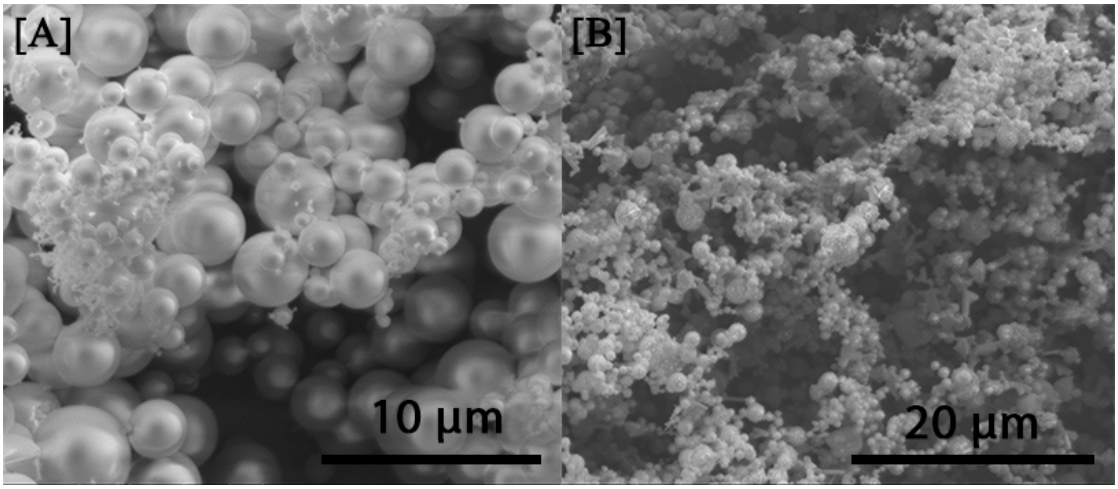

Figure 12. Micrographs of the depositions made on the copper coupon in (A) oxidizing less humid and (B) inert less humid conditions. Image (A) has a slight difference in the dark/light contrast of the particles and, therefore only appears to be different.

For the depositions on the copper coupon, the micrographs can be seen in

Figure 12. Image A shows the deposition from the oxidizing conditions and the main shape of the particles was smooth spheres, with very small amounts of non-spherical particles. In second image (B in Figure 12), the deposition made under inert conditions can be observed. The particles constituting this deposition were found to have spherical nubby shapes. Moreover, rectangular and spike shaped objects were also present in the deposition. No chemical interaction with the copper surface was observed in micrographs A and B.

From these results it is indicated that during oxidizing conditions, the deposition of tellurium onto these surfaces will not be affected by the underlying surface of aluminum, zinc and copper, as the morphology of the particle constituting the deposition remained the same. Nor will any chemical interaction occur at the conditions of these experiments. Moreover, as no strong attachment was observed for any of the metal surfaces and the formed deposition it is possible that revaporization of the tellurium will occur, should the conditions change (e.g. increases in temperature, gas flows). Alternatively, as the method designed to reduce radionuclide release in the containment is the containment spray [15], these depositions could be washed down into the containment sump.

For the depositions made in inert conditions, lack of surface attachment of the deposition to the underlying metal surfaces was again observed. Moreover, the shapes of the particles of which the depositions consist were similar for the depositions on the aluminum and zinc coupons. However, for the deposition made on the copper surface, the smooth spherical particles had partially been replaced by spherical nubby particles.

For clarity, it is important to note that these coupon surfaces seen in Figures 10,11 and 12 were positioned horizontally to the flow during the experiments. Therefore, gravimetrical settling contributed to the formation of these depositions. However, should the surface be located vertically to the surface of the coupon this could affect the formation of these deposit. Still, during the analysis of these surfaces, neither turning the surface to the side nor exposing it to the high vacuum damaged the deposition. However, using a paper tissue removed all visual traces of the depositions completely.

4.1.2 Chemical speciation, XRD

The next step was verification of the chemical composition of the deposits shown in Figures 10, 11 and 12. For this investigation, glancing angle XRD was used and the resulting spectra for all deposits on the aluminum coupons can be found in Figure 13, the deposits on the zinc coupons are shown in Figure 14 and the deposits on the copper coupons can be seen in Figure 15. In each figure three spectra can be seen. These represent, starting from the top: the underlying surface (black, e.g. aluminum, zinc or copper) and then the depositions formed; under

inert conditions with increased humidity (orange), under inert conditions (purple), under oxidizing conditions with increased humidity (green), and under oxidizing conditions (blue). All peaks that have been identified in these spectra have been assigned the identification suggested by the database used. To avoid cluttering the spectra, when a peak exists in multiple spectra only the top spectrum is assigned the identification.

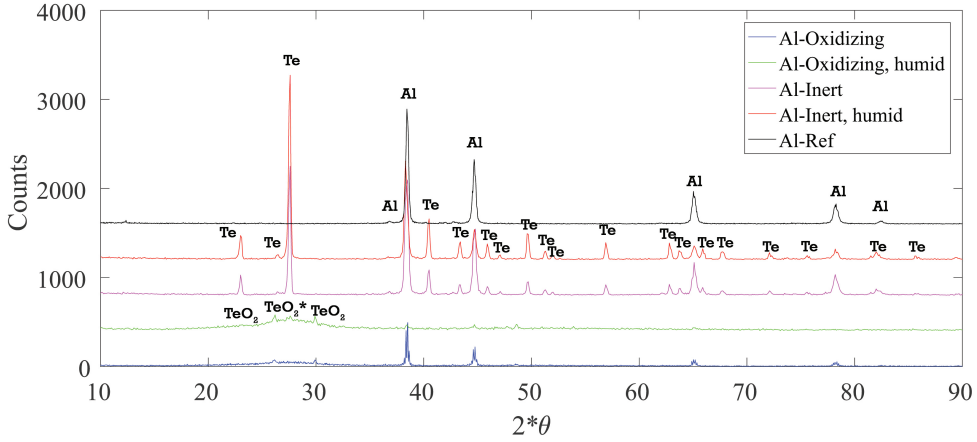

Figure 13. The results from X-ray diffraction (XRD) analysis, with a glancing angle of 5°, of the depositions made on the aluminum coupon under oxidizing humid (green), oxidizing (blue), inert humid (orange) and inert (purple) conditions. The black spectrum represents an analysis made on a clean aluminum coupon surface. Each peak has been indicated with the identification made through the software used in conjunction with the XRD equipment. Some spectra have been scaled to fit in the figure.*TeO_2 is indicated by the database to have a different crystal structure than for the two peaks indicating TeO_2.

The chemical speciation of the deposition made on the aluminum coupon can be seen in Figure 13. What can be observed is that, under oxidizing conditions both with (green) and without (blue) increased humidity, a bulge appears between 25°and 35°(2θ). Moreover, this bulge contains two peaks for non-increased humid oxidizing conditions and three peaks when the humidity has been increased. All have been positively matched to TeO_2. However, for the middle peak the crystal structure corresponded to orthorhombic and the other two TeO_2 paratellurite. When the experiment was done under inert conditions with (orange) and without (purple) increased humidity, no significant difference was observed between the spectra. The chemical composition was positively matched to Te. The final spectrum (black) shows an analysis of the underlying surface of aluminum.

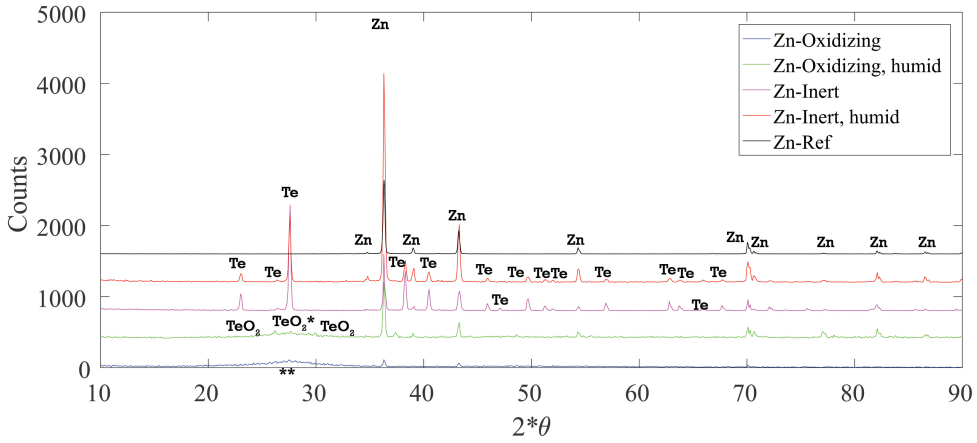

Figure 14. The results from X-ray diffraction (XRD) analysis, with a glancing angle of 5°, of the depositions made on the zinc coupon under oxidizing humid (green), oxidizing (blue), inert humid (orange) and inert (purple) conditions. The black spectrum represents an analysis made on a clean zinc coupon surface. Each peak has been indicated with the identification made through the software used in conjunction with the XRD equipment. Some spectra have been scaled to fit in the figure."*TeO_2" is indicated by the database to have a different crystal structure than the two peaks indicating TeO_2."**"no peaks were observed in this bulge.

The results of the chemical speciation by XRD, when a zinc coupon was used as an underlying surface, can be seen in Figure 14. For the oxidizing conditions, both with (green) and without (blue) humidity, between 25°and 35°(2θ) a bulge appears. When less humidity is used, it appears that there are no peaks in it (e.g. unlike the aluminum coupon case). However, under oxidizing conditions with increased humidity there are three peaks appearing. These were positively matched as all belonging to TeO_2, but the middle peak corresponded to the orthorhombic crystal structure and the other two to the paratellurite. The other two spectra (excluding the black) correspond to inert conditions with (orange) and without (purple) increased humidity. In these two spectra no significant difference can be observed between the chemical composition of the depositions and the main identification was Te. A analysis of a clean surface of zinc is shown in the black spectrum.

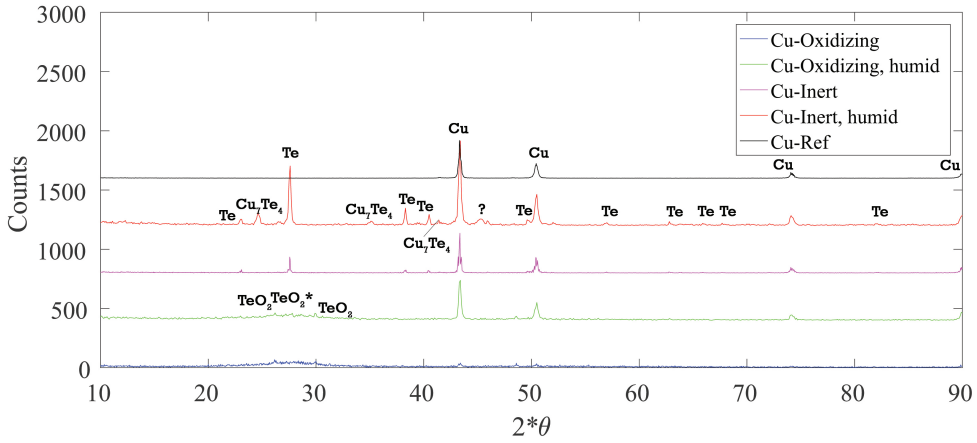

Figure 15. The results from X-ray diffraction (XRD) analysis, with a glancing angle of 5°, of the depositions made on the copper coupon under oxidizing humid (green), oxidizing (blue), inert humid (orange) and inert (purple) conditions. The black spectrum represents an analysis made on a clean copper coupon surface. Each peak has been indicated with the identification made through the software used in conjunction with the XRD equipment. Some spectra have been scaled to fit in the figure. "*TeO_2"is indicated by the database to have a different crystal structure than the two peaks indicating TeO_2. The peaks marked "?" were not positively identified.

The chemical speciation of the deposition on the copper surfaces can be seen in Figure 15. The spectra corresponding to oxidizing conditions with (orange) and without (purple) increased humidity shows that between 25°and 35°(2θ) three peaks are visible for the increased humidity and two for the non-humid conditions. These have been positively matched to correspond to TeO_2, the middle peak corresponding to the orthorhombic and the other two the paratellurite crystal structure. When the inert conditions with (orange) and without (purple) increased humidity were investigated, the results showed that under both conditions tellurium was part of the deposition. However, when increasing the humidity there were peaks that were positively matched as Cu_7Te_4 and one that was not identified.

Observing the results in figures 13, 14 and 15, it can be seen that the underlying metal did not have considerable effect on the chemical speciation of the deposition for either of the two oxidizing conditions. For the two oxidizing conditions, two potential crystal structures of TeO_2 were observed when the humidity was increased, and only one when humidity was lacking. The paratellurite of TeO_2 seen in both spectra can be formed when oxygen reacts with Te [42] (Equation 5) and therefore this reaction could be the source of the paratellurite TeO_2. As the orthorhombic crystal structure only appeared when the humidity was increased, the humidity could have affected the gas phase chemical speciation. In the literature [19, 30, 31, 32] it has been reported that under oxidizing conditions, when steam is present at high temperature, that the transient compound $TeO(OH)_2$ is formed. Thus,

a potential explanation could be that when $TeO(OH)_2$ reverts back to TeO_2, as temperature drops, it adopts the orthorhombic structure. From a chemical standpoint, the crystal structure matters little for TeO_2 as it is dimorphic [42]. However, the formation of $TeO(OH)_2$ could have an impact on the source term evaluation of tellurium as it enhances the volatility of TeO_2 [30]. Thus, proving that it exists as a transient species would be important. Still, these experiments only give an indication that increasing the humidity alters the TeO_2 crystal structure of the deposition and does not explicitly affect the gas phase TeO_2.

Furthermore, the results for the inert conditions with and without increased humidity in figures 13, 14 and 15 shows that when humidity was low, the underlying metal surface did not affect the chemical speciation of the deposition, as only the crystal structure of Te was observed in these spectra. For the aluminum and zinc surface under inert conditions with increased humidity, the spectra were similar to the experiment lacking humidity as no new chemical species was observed. However, for the deposition on the copper surface new peaks emerged under inert conditions with increased humidity. In total, five new peaks emerged and three of these were positivity matched to Cu_7Te_4 and the other two remain unknown. This is an indication that tellurium reacted below 339 K under inert humid conditions with the copper surface. This is reported to be a possibility in the literature [22, 35], where it is stated that tellurium, when steam is present, could react with metal surfaces in the containment. However, more experiments, both with and without humidity, are needed for clarification.

4.1.3 Chemical speciation, XPS

As a complement to the XRD, XPS was used on one of the depositions. The chosen deposition was the one made on the zinc coupon under oxidizing conditions without humidity, as no identification of anything else than zinc was achieved with XRD. In this part of the work, only the focused scan can be found as it is in it that the chemical identification will be given. The rest can be seen in Appendix A. The spectrum can be seen in Figure 16.

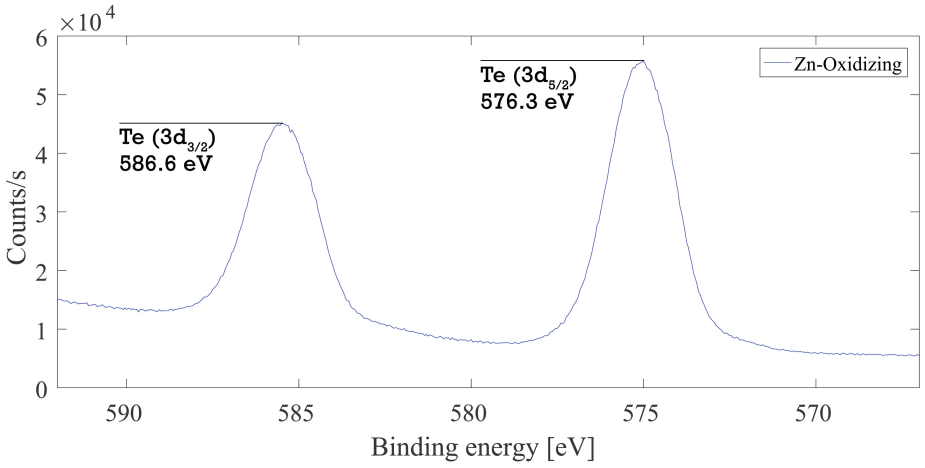

Figure 16. The focused spectrum produced by X-ray photoelectron spectroscopy of the deposition made on the zinc coupon under oxidizing conditions. Two peaks can be seen, one at 586.6 eV ($3d_{3/2}$) and the second at 576.3 eV ($3d_{5/2}$). Based on the literature, these have been correlated to tellurium [46].

Two peaks can be observed in Figure 16, located at binding energies of 586.6 eV and 576.3 eV. In the literature [46], the closest tellurium species with energies close to these is TeO_2. The reported values for TeO_2 are 586.5±0.2 eV for the $3d_{3/2}$ and 576.1±0.2 eV $3d_{5/2}$.

The results observed in Figure 16 indicate that the deposition made under oxidizing conditions on the zinc surface contains TeO_2. Comparing this to the XRD data for the zinc surface in Figure 14 (blue spectrum), it is possible that this bulge corresponds to tellurium dioxide. However, the peaks seen in the XRD spectrum in Figure 14 are not visible.

4.2 Tellurium interaction with sea-salt

The experimental results from the TGA analysis can be observed in Figure 17 for inert conditions and Figure 18 for oxidizing conditions. In these, several lines can be seen and these represent either one of the mixture ratio samples (S1 red, S2 pink, and S3 black), or the references (Ref1 green and Ref2 blue). All the weights have been normalized towards the first measured value by the TGA. These lines are the average outcome of the three replicates made for each sample.

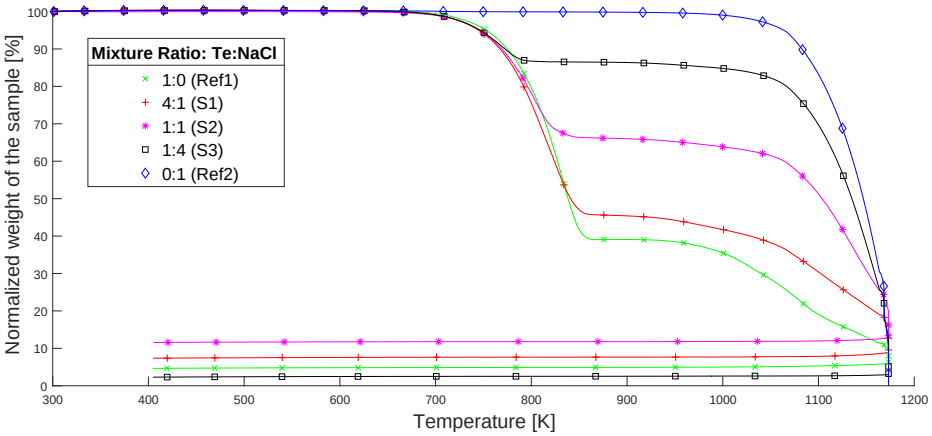

Figure 17. The thermogravimetric analysis results for the different Te:NaCl-ratios (weight basis) heated in inert conditions. The different lines represent the average of three replicates of 0:1 (Ref1, blue diamonds), 1:4 (S1, black squares), 1:1 (S2, pink stars), 4:1 (S3, red pluses) and 1:0 (Ref2, green crosses) of tellurium and sodium chloride, respectively. All weights have been normalized towards the first measured weight (8-9 mg) by thermogravimetric analysis. The measuring interval was one second.

The results for inert conditions can be seen in Figure 17. For all samples and the tellurium reference, the masses remain unchanged until 690-710 K. At these temperatures, the first mass loss for all the samples and the tellurium reference can be observed. These mass losses continue until temperatures of 780-860 K, when the mass losses stop, depending on the tellurium content (as more of it in the sample prolongs the mass loss). After these temperatures, the mass loss significantly slows down. Again, depending on the content of tellurium, the rate of the mass loss differs (shorter for the samples with more tellurium). At temperatures between 920-1080 K, the second mass losses occur for all samples and both references (the sodium chloride reference has been unaffected until these temperatures are reached). However, the tellurium content is again the main dictating parameter for the temperature at which the mass loss starts for the samples. These mass losses continue until the end of the experiment, ending at a normalized mass of 5 % for Ref1, 7.6 % for S1, 12 % for S2, 2.5 % for S3 and almost no mass loss for Ref2, compared to the original values.

What is most likely happening when the temperature increases are that tellurium is being volatilized during the first mass losses of the samples. Considering that at the same temperatures that these mass losses occur at, the tellurium reference is also experiencing a mass loss, it is possible that the tellurium part of the samples was volatilized. Moreover, as the melting point of tellurium (725 K [42]) is roughly at the temperatures of these mass losses, a phase change is occurring for the tellurium. Possible tellurium candidates that could be formed during these

mass losses are Te or Te_2 [22]. The normalized mass after the first mass loss can be correlated to the content of sodium chloride in the sample, e.g. more sodium chloride results in a higher normalized mass after the first mass loss. During the subsequent mass losses, the samples are experiencing a combined mass loss of both tellurium (as indicated by the tellurium reference mass loss) and the sodium chloride (as indicated by the sodium chloride reference mass loss). Moreover, at the temperature when the second mass loss occurs, the sodium chloride also undergoes a phase change as the melting point (1074 K [42]) has been reached.

Thus, from Figure 17 it can be concluded that nothing happens between the tellurium and sodium chloride, as they remain in the pan. This is based on the similarity between the samples, as well as that the main part (e.g. tellurium or sodium chloride) of the sample dictates the behavior of the sample. The latter conclusion is based on the similarity between sample S1 (mainly tellurium) to the tellurium reference and sample S3 (mainly sodium chloride) to the sodium reference. However, these results do not exclude a gas phase interaction between the tellurium and sodium chloride, but such a reaction would not be visible in the TGA results.

Nevertheless, it is still possible that if tellurium would remain until a higher temperature is reached (e.g. by being trapped in the cladding [25, 26, 27]), it could be possible that a reaction between the tellurium and sodium chloride could occur.

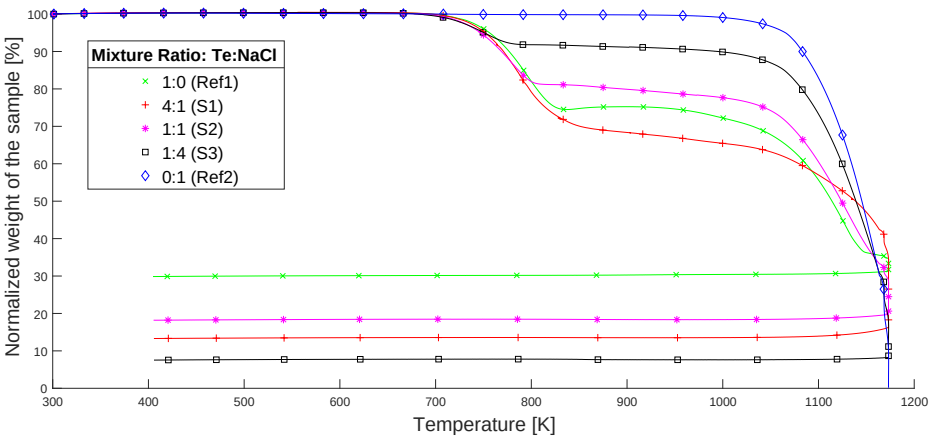

Figure 18. The thermogravimetric analysis results for the different Te:NaCl-ratios (weight basis) heated in oxidizing conditions. The different lines represent the average of three replicates of 0:1 (Ref1, blue diamonds), 1:4 (S1, black squares), 1:1 (S2, pink stars), 4:1 (S3, red pluses) and 1:0 (Ref2, green crosses) of tellurium and sodium chloride, respectively. All weights have been normalized towards the first measured weight (8-9 mg) by thermogravimetric analysis. The measuring interval was 1 second.

The results for oxidizing conditions can be seen in Figure 18. For all samples, the masses remain unchanged until 680-710 K. At these temperatures, the first mass losses for all samples can be seen. The changes continue until 780-850 K. Similar to the inert conditions experiments, these mass losses continue until different normalized masses are reached, which correlates to the tellurium content of the samples (e.g. mass loss continues for longer for the samples with more tellurium). After these temperatures, the mass loss starts to slow down. For the samples S1 and S2, the rate of the mass change is slower, but is still noticeable. For S3 (the sample with the most sodium chloride) the mass loss rate is very small and barely changes the mass. Between 1000-1050 K, all samples experience a noticeable mass decrease that is maintained until the end of the experimental run, ending at normalized masses of the original value: of 18 % for S1, 18 % for S2 and 8 % for S3.

Observing the references for oxidizing conditions in Figure 18, the sodium chloride (Ref2) has no observed mass loss until 1001-1047 K. After this, mass loss occurs rapidly and continues until the end of the experiment, where almost no mass remains. At the same time, the tellurium reference (Ref1) is partially behaving as S1, S2, and S3 in Figure 18, i.e., initially the normalized mass remains unchanged until 680-710 K and then a mass loss occurs. However, the divergence from the samples S1, S2 and S3 occurs at 780-850 K, where the tellurium reference is starting to gain mass instead of the slower rates of mass losses of S1 and S2 and the almost unchanged mass of S3. This continues until 1001-1047 K, where instead the mass increase becomes a mass loss. This, mass loss remains until the end of the experiment and ends at a 30% normalized mass of the original value.

Similar to the experiments carried out under inert conditions, none of the samples lose any mass until temperatures of 680-710 K. Moreover, these temperatures are close the melting point of tellurium (725 K [42]) and also TeO (643 K [40]). Thus, at these temperatures one or several phase changes are occurring in the sample. Considering that the tellurium reference is also experiencing a mass loss at these temperatures, it is possible that what could be volatilized is either tellurium vapor (similar to the inert conditions experiments) or a tellurium oxide species (considering oxidizing conditions).

Following the first mass loss for the tellurium reference is a mass increase. This is not observed for any of the other samples or the sodium chloride reference. The increase in mass of the tellurium reference can be attributed to potential oxidation (likely only on the surface) of the tellurium to α-TeO_2. The arguments for this can be found in a Te-O phase diagram [47], as decreasing the amount of tellurium would shift, at these temperatures, towards the vertical line of α-TeO_2. Moreover, these temperatures are close to the melting point of TeO_2 (1006 K [40]). Therefore, a phase change is most likely occurring at these temperatures. The phase diagram

of Te-O [47] indicates that above the melting point of TeO_2, both liquid and gas phases exist. Considering this, the explanation for the second mass loss for the tellurium reference would be volatilization of TeO_2.

Comparing the tellurium reference and the different samples, it is clear that no mass increases are observed for the samples. Thus, this is indicative that sodium chloride in the sample is preventing the mass increase. The first potential explanation could simply be that the sodium chloride is physically preventing the oxidization of tellurium in the pan by forming a top layer of sodium chloride on the surface. Alternatively, a potential chemical reaction could be occurring between the tellurium and sodium chloride that either prevents the oxidization of tellurium or surpasses the mass increase caused by oxidization.

The difference between the three samples are minor and can be explained by the content of sodium chloride. Increasing the sodium chloride content, consequently increases the similarity to the sodium chloride reference. Thus, even a small amount of sodium chloride (in this case, a fourth of the weight of the tellurium) affects the volatilization of tellurium.

Based on the observations in Figure 18, a number of furnace experiments were performed, to gain a better insight into what was happening during the TGA experiments under oxidizing conditions. Primarily the intention was to determine if something happens and not only volatilization of the individual parts. This was done for a ratio of 1-1 of tellurium and sodium chloride. The results can be seen in Figure 19. The first image (A), resembles the initial appearance of the state of the samples; the black part is tellurium (black powder) and the white part sodium chloride (white powder).

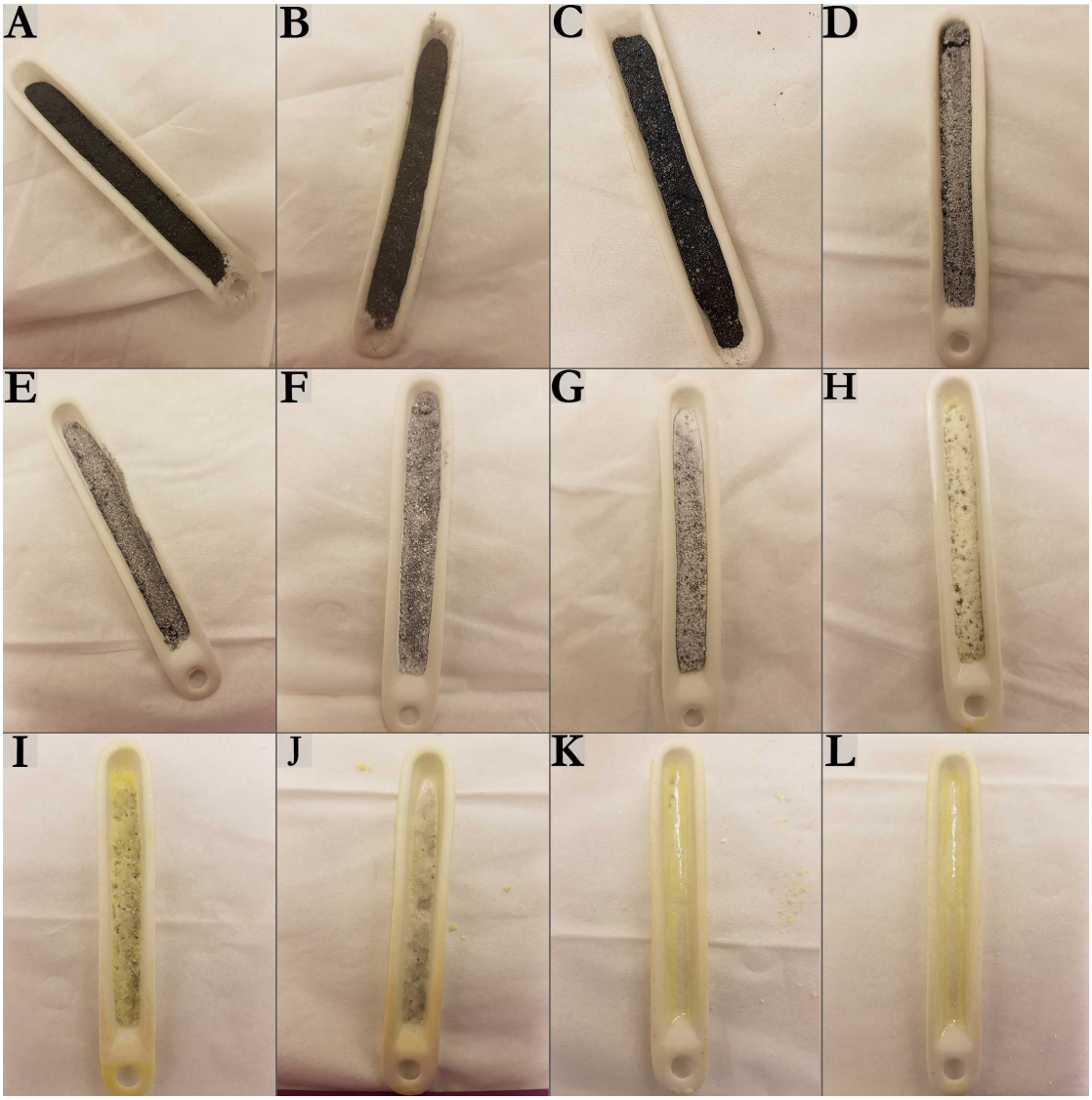

Figure 19. Crucibles containing the sample, as seen after the furnace experiment. Initial composition of the samples was 1:1 of tellurium and sodium chloride (2 g). In total eight, temperatures were investigated: (A) 473 K, (B) 573 K, (C) 623 K, (D) 673 K, (E) 723 K, (F) 773 K, (G) 823 K, (H) 873 K, (I) 923 K, (J) 973 K, (K) 1023 K and (L) 1073 K.

The outcome of the furnace experiments can be seen in Figure 19. These images show mixtures of the same ratio that have been heated to different temperatures and then allowed to cool. What can be seen is that the sample remains unchanged up to 673 K (D), as in this sample white particles have emerged. Up to 823 K (G), the white particles are increasingly becoming more visible in the sample, most likely due to reduced amounts of black powder. However, at 873 K (H) the first notable difference can be observed. A yellow phase has emerged and covers the

mixture as well as the crucible. At the following temperature of 923 K (i), the yellow phase has become more prevalent and the white particles have started to lose their initial shape. On heating to 973 K (J), the sample drastically changes, as it melts and has noticeably lost volume. Beyond 1023 K (K and L), only the yellow phase remains, as a glaze covering the crucible.

In the first images (A to C) in Figure 19, minor changes to the samples can be observed. Considering the content of tellurium (black particles) and sodium chloride (white particles), the lack of change is consistent with the melting points of tellurium (725 K [42]) and sodium chloride (1074 K [42]). At 673 K, the reason for the appearance of the white particles is not clear, based on these images alone. However, above 723 K the melting point of tellurium has been reached[8]. Thus, reaching the melting point could potentially result in minor volatilization of the tellurium in the sample. Observing the sample heated to 873 K (H) a yellow phase has emerged. In the literature [42], two potential chemical compounds consisting of tellurium, oxygen, sodium, and chloride can be found that have this yellow color. These are $TeCl_4$ which has a pale-yellow color, and the yellow TeO_2 (orthorhombic). Of these, only $TeCl_4$ has a melting point and boiling point below 1000 K [40]. Moreover, as the melting point and boiling point of sodium chloride are 1074 K [40] and 1686 K [40], respectively, no phase change should occur that could alter the appearance. However, at a temperature of 1023 K (K) nothing remains of the sample in the crucible. This is indicative that something has formed that has either removed the sodium chloride, or a reaction has occurred where something more volatile than sodium chloride has been formed.

Comparing the results from the TGA under oxidizing conditions in Figure 18 and furnace experiments in Figure 19, the changes occurring during the two mass losses can be observed. During the first mass loss in Figure 18 for sample S2, only the black part of the sample is seemingly disappearing in Figure 19 images D to G. Thus, it can be concluded that it is the decreasing amount of black powder that is the cause of the mass loss.

The sample heated to 873 K, seen as image H in Figure 19 shows a yellow phase emerging. At the same time in the TGA result in Figure 18 for the sample S2, a slow mass loss is occurring at this temperature. Thus, potentially what is volatilized is this yellow phase or the species that form it when cooled down, considering that the yellow phase covers the crucible and the mixture. At temperatures 923 K and 973 K, respectively, the sample is slowly changing its appearance and melting. Observing the TGA result of samples S2 in Figure 18 at the same temperature, no drastic changes occur between these samples, indicating that the species being volatilized remain the same at these temperatures. Above 1023 K,

[8] Attempts where made by SEM/EDX to determine the chemical composition. However, this was not successful due to the shape of the crucible.

nothing except the yellow glaze remains in the crucible. The TGA result (S2) at the same temperature in Figure 18, shows a mass loss of the sample, the tellurium and the sodium chloride reference. However, the sodium chloride reference is only beginning to lose mass whereas the other two are showing significant mass losses. Considering that sodium chloride has a boiling point of 1686 K [40], a rapid loss of sodium chloride at these temperatures would not be expected. This indicates that something has interacted with the sodium chloride and formed a more volatile compound.

5 Conclusions

In this work, experiments were carried out to determine the behavior of tellurium with surfaces found in the containment under different conditions. When tellurium was oxidized under less humid conditions and then transported to surfaces of aluminum, zinc and copper surfaces, no chemical interaction was observed only deposition. Micrographs of these deposits showed that they consisted mainly of smooth spherical particles with minor amounts of other shapes. The deposits were determined to compose of the paratellurite crystal structure of TeO_2. When the humidity was increased, the crystal structure of orthorhombic TeO_2 was seen. Thus, indicating that something changed when the humidity was increased. Possibly explained by the formation of a transient compound, e.g. $TeO(OH)_2$.

If tellurium entered the containment without being oxidized (e.g. inert conditions), little evidence was found that tellurium reacts with the aluminum, zinc or copper surfaces; instead, deposits were formed. In all the deposits, spherical, rectangular and spike shaped particles were found. However, on the copper surface nubby particles were also observed. The chemical speciation showed that metallic-Te was the main compound. If tellurium entered the containment under inert humid conditions, the outcome was similar to the inert conditions for the aluminum and zinc surfaces. However, for the copper surface indications where found that a reaction occurred where possibly Cu_7Te_4 was formed.

In the end, no strong attachment was observed for most deposits. The only exception was the copper surface interaction with tellurium under inert humid conditions. Thus, revaporization is likely

The second part of this work concerns the use of seawater as a potential coolant and its effect on the tellurium source term. It was seen by TGA that under inert conditions the sodium chloride would not affect the tellurium at temperatures below 1073 K in the solid-solid, liquid-liquid phases, or the interfaces of these. However, some issues were seen as considerable amounts of tellurium had volatilized before reaching the melting point of sodium chloride. Thus, potentially too little tellurium might have remained for a reaction to take place.

Instead, during oxidizing conditions it was seen that a mass increase that occurred for the reference did not occur for the samples. Thus, two potential explanations were proposed: either the sodium chloride physical prevented the oxidation of tellurium or a reaction occurred between the tellurium and the sodium chloride. To determine if something actually happened between the tellurium and the sodium chloride, these were heated in a furnace to a range of selected temperatures. From these experiments, it was observed that (1) a yellow phase emerged, (2) the sample formed a melt before the melting point of sodium chloride and (3) the sample was completely consumed before reaching the melting point of sodium chloride.

6 Future work

For the containment experiments, reducing conditions would be of interest as this is one of the conditions expected to occur during a nuclear accident. Moreover, investigating the interaction with painted surfaces would also be relevant, as painted surfaces have been pointed out in the literature to have a potential for considerable effect on the tellurium source term. Considering the lack of reaction with the metals observed (except copper), the chemistry of tellurium in sump water is highly relevant as it can be expected that most of the tellurium will be washed down into this water. Finally, more experiments to verify the interaction under inert humid conditions between tellurium and copper is needed.

Considering the very limited scope of this part in this work, more work could also be performed on the seawater effects on tellurium (and other fission products). The observed yellow phase could be furthered examined to determine the elemental composition of it and possibly the chemical species. The water chemistry that would be the result of using seawater could potentially have considerable effects on all fission products. Not only, as in this work, are the effects of sodium chloride, but the potential carbon related content of seawater is also of interest.

7 Acknowledgements

This work was founded by the APRI-9 (Accident Phenomena of Risk Importance).

A great deal of thanks are extended to:

My supervisor Christian Ekberg for his willingness, knowledge and patience to help with this work.

Henrik Glänneskog for creating order among the senior academics and providing insight and knowledge into the field of severe nuclear accidents.

Mark Foreman, for his ideas and expertise of nuclear accidents.

My examiner Britt-Marie Steenari.

To Burcak Erbin, for your invaluable help with the experiments and your willingness to answer questions and help out, even if you do not need to or have time for it.

To the rest of the people at NC/IMR, that occasionally endures me. Among these Marino Gergoric should be mentioned specifically. **As** we had way too much chit chat, not to.

Till sist, men ändock viktigast: min familj och vänner, vet inte vad jag hade gjort utan er.

References

[1] E.C. European Commission. *Communication From the Commission to the European Parliment and the Council: European Energy Security Strategy.* 2014. URL: http://eur-lex.europa.eu/legal-content/EN/TXT/?uri=CELEX\%3A52014DC0330,2018-03-15.

[2] B. Clément and R. Zeyen. "The objectives of the Phébus FP experimental programme and main findings". In: *Annals of Nuclear Energy* 61 (2013). Special Issue : Phebus FP Final Seminar, pp. 4 –10. ISSN: 0306-4549.

[3] T. Haste, F. Payot, C. Manenc, B. Clément, Ph. March, B. Simondi-Teisseire, and R. Zeyen. "Phébus FPT3: Overview of main results concerning the behaviour of fission products and structural materials in the containment". In: *Nuclear Engineering and Design* 261 (2013), pp. 333 –345. ISSN: 0029-5493.

[4] P. March and B. Simondi-Teisseire. "Overview of the facility and experiments performed in Phlébus FP". In: *Annals of Nuclear Energy* 61 (2013). Special Issue : Phebus FP Final Seminar, pp. 11 –22. ISSN: 0306-4549.

[5] Y. Pontillon, G. Ducros, and P.P. Malgouyres. "Behaviour of fission products under severe PWR accident conditions VERCORS experimental programme—Part 1: General description of the programme". In: *Nuclear Engineering and Design* 240.7 (2010), pp. 1843 –1852. ISSN: 0029-5493.

[6] Y. Pontillon and G. Ducros. "Behaviour of fission products under severe PWR accident conditions: The VERCORS experimental programme—Part 2: Release and transport of fission gases and volatile fission products". In: *Nuclear Engineering and Design* 240.7 (2010), pp. 1853 –1866. ISSN: 0029-5493.

[7] Y. Pontillon and G. Ducros. "Behaviour of fission products under severe PWR accident conditions. The VERCORS experimental programme—Part 3: Release of low-volatile fission products and actinides". In: *Nuclear Engineering and Design* 240.7 (2010), pp. 1867 –1881. ISSN: 0029-5493.

[8] H. Glänneskog. *Iodine-Metal Surface Interactions under Severe Accident Conditions in a Nuclear Power Plant.* (Doctoral thesis at Chalmers University of Technology. No. 2374). Institution of Chemistry and Chemical Engineering, Chalmers University of Technology, 2005. ISBN: 91-7291-692-3.

[9] J. Holm. *Investigation of the behaviour of gaseous I2 and RuO4 in different atmospheres.* (Licenciate thesis at Chalmers University of Technology. No. 2009:10). Institution of Chemistry and Chemical Engineering, Chalmers University of Technology, 2009.

[10] S. Tietze. *The chemistry of organic iodides under severe nuclear accident condtions in LWRs*. (Doctoral thesis at Chalmers University of Technology. No. 3839). Institution of Chemistry and Chemical Engineering, Chalmers University of Technology, 2015. ISBN: 978-91-7597-158-2.

[11] I. Kajan. *Transport and Containment Chemistry of Ruthenium under Severe Accident Conditions in a Nuclear Power Plant*. (Doctoral thesis at Chalmers University of Technology. No. 4145). Institution of Chemistry and Chemical Engineering, Chalmers University of Technology, 2016. ISBN: 978-91-7597-464-4.

[12] Internation Atomic Energy Agency. *International Nuclear and Radiological Event Scale (INES)*. 2017. URL: https://www.iaea.org/topics/emergency-preparedness-and-response-epr/international-nuclear-radiological-event-scale-ines,2018-03-13.

[13] N.A. Beresford and J. Smith. *Chernobyl: Catastrophe, Consequences and Solutions*. Berlin Heidelberg: Springer- Verlag, 2005. ISBN: 3-540-23866-2.

[14] World Nuclear Association. *Fukushima Accident*. 2017. URL: http://www.world-nuclear.org/information-library/safety-and-security/safety-of-plants/fukushima-accident.aspx,2018-03-10.

[15] G. Ducros. "Fission Product Release and Transport". In: *Nuclear Safety in Light Water Reactors: Severe Accident Phenomenology*. Ed. by B.R. Sehgal. 1st ed. Elsevier, 2012. Chap. 5, pp. 426–517. ISBN: 9780123919069.

[16] G. Choppin, J.O. Liljenzin, J. Rydberg, and C. Ekberg. "Chapter 21 - The Nuclear Fuel Cycle". In: *Radiochemistry and Nuclear Chemistry (Fourth Edition)*. Ed. by G. Choppin, J.O. Liljenzin, J. Rydberg, and C. Ekberg. Fourth Edition. Oxford: Academic Press, 2013, pp. 685–751. ISBN: 978-0-12-405897-2.

[17] G. Choppin, J.O. Liljenzin, J. Rydberg, and C. Ekberg. "Chapter 19 - Principles of Nuclear Power". In: *Radiochemistry and Nuclear Chemistry (Fourth Edition)*. Ed. by G. Choppin, J.O. Liljenzin, J. Rydberg, and C. Ekberg. Fourth Edition. Oxford: Academic Press, 2013, pp. 595–653. ISBN: 978-0-12-405897-2.

[18] J. Katakura. *JENDL FP decay Data File 2011 and Fission Yields Data File 2011*. Report. JAEA-Data/Code 2011-025. Division of Nuclear Data, Reactor Engineering, Nuclear Scienece, and Engineering Directorate, 2011.

[19] A. Alonso and C González. *f the chemical behaviour of tellurium species in the reactor pressure vessel and the reactor cooling system under severe accident conditions*. Report. EUR–13787. Commission of the European Communities (CEC), The Joint Research Centre, 1991.

[20] J. Magill, G. Pfenning, R. Dreher, and Z. Sòti. *Karlsruher Nuklidkarte, 9 Edition*. 2015.

[21] H. Kleykamp. "The Chemical State of the Fission Products in Oxide Fuels". In: *Journal of Nuclear Materials* 131.2 (1985), pp. 221–246. ISSN: 0022-3115.

[22] J. McFarlane. "Fission product tellurium chemistry from fuel to containment". In: *Proceedings of the Fourth CSNI Workshop on the Chemistry of Iodine in Reactor Safety* (1996). (PSI–97-02). Guentay, S. (Ed.). Switzerland, pp. 563–585.

[23] L. Desgranges, Ch. Riglet-Martial, I. Aubrun, B. Pasquet, I. Roure, J. Lamontagne, and T. Blay. "Evidence of tellurium iodide compounds in a power-ramped irradiated UO2 fuel rod". In: *Journal of Nuclear Materials* 437.1 (2013), pp. 409 –414. ISSN: 0022-3115.

[24] S. Imoto and T. Tanabe. "Chemical state of tellurium in a degraded LWR core". In: *Journal of Nuclear Materials* 154.1 (1988), pp. 62 –66. ISSN: 0022-3115.

[25] R. de Boer and E.H.P. Cordfunke. "Reaction of tellurium with Zircaloy-4". In: *Journal of Nuclear Materials* 223.2 (1995), pp. 103 –108. ISSN: 0022-3115.

[26] R. de Boer and E.H.P. Cordfunke. "The chemical form of fission product tellurium during reactor accident conditions". In: *Journal of Nuclear Materials* 240.2 (1997), pp. 124 –130. ISSN: 0022-3115.

[27] J.L. Collins, Morris F. Osborne, and R. A. Lorenz. "Fission Product Tellurium Release Behavior Under Severe Light Water Reactor Accident Conditions". In: *Nuclear Technology* 77.1 (1987), pp. 18–31.

[28] I Johnson and C.E. Johnson. "Mass spectrometry studies of fission product behavior: I. Fission products released from irradiated LWR fuel". In: *Journal of Nuclear Materials* 154.1 (1988), pp. 67 –73. ISSN: 0022-3115.

[29] K. Pettersson, H. Chung, M. Billone, T. Fuketa, F. Nagase, C. Grandjean, G. Hache, J. Papin, L. Heins, Z. Hozer, J. In de Betou, S. Kelppe, R. Mayer, H. Scott, J. Voglewede, H. Sonnenburg, S. Sunder, M. Valach, V. Vrtilkova, N. Waeckel, W. Wiesenack, and M. Zimmermann. *Nuclear Fuel Behaviour in Loss-of-coolant Accident (LOCA) Conditions*. Report. (NEA–6846). Division of Nuclear Data, Reactor Engineering, Nuclear Scienece, and Engineering Directorate, 2009.

[30] A. P. Malinauskas, J. W. Gooch Jr., and J. D. Redman. "The Interaction of Tellurium Dioxide and Water Vapor". In: *Nuclear Applications and Technology* 8.1 (1970), pp. 52–57.

[31] W. A. Dutton and W. Charles Cooper. "The Oxides and Oxyacids of Tellurium". In: *Chemical Reviews* 66.6 (1966), pp. 657–675.

[32] R.J.M. Konings, E.H.P. Cordfunke, and V . Smit-Groen. "The vapour pressures of hydroxides II. TeO(OH)2". In: *The Journal of Chemical Thermodynamics* 22.8 (1990), pp. 751 –756. ISSN: 0021-9614.

[33] E.A. Maugeri, J. Neuhausen, R. Eichler, D. Piguet, and D. Schumann. "Thermochromatography study of volatile tellurium species in various gas atmospheres". In: *Journal of Nuclear Materials* 452.1 (2014), pp. 110 –117. ISSN: 0022-3115.

[34] R.A. Sallach, C.J. Greenholt, and A.R. Taig. *Chemical interactions of tellurium vapors with reactor materials*. Report. NUREG/CR–2921. Sandia National Labs., Albuquerque, NM (USA), 1984.

[35] E.C. Beahm. *Tellurium behavior in containment under light water reactor accident conditions*. Report. NUREG/CR–4338. Oak Ridge National Lab., TN (USA), 1986.

[36] P.D.W. Bottomley, K. Knebel, S.V. Winckel, T. Haste, S.M.O. Souvi, A. Auvinen, J. Kalilainen, and T. Kärkelä. "Revaporisation of fission product deposits in the primary circuit and its impact on accident source term". In: *Annals of Nuclear Energy* 74 (2014). ERMSAR 2013 conference of the SARNET network, pp. 208–223. ISSN: 0306-4549.

[37] H. Glänneskog. "Interactions of I_2 and CH_3I with reactive metals under BWR severe-accident conditions". In: *Nuclear Engineering and Design* 227.3 (2004), pp. 323 –329. ISSN: 0029-5493.

[38] "Composition of Seawater and Ionic Strength at Various Salinities". In: *CRC Handbook of Chemistry and Physics*. 98th Edition (Internet Version 2018).

[39] Y. Kanai. "Geochemical behavior and activity ratios of Fukushima-derived radionuclides in aerosols at the Geological Survey of Japan, Tsukuba, Japan". In: *Journal of Radioanalytical and Nuclear Chemistry* 303.2 (2015), pp. 1405–1408. ISSN: 1588-2780.

[40] "Physical Constants of Inorganic Compounds". In: *CRC Handbook of Chemistry and Physics*. 98th Edition (Internet Version 2018).

[41] 2012. "Tellurium and its inorganic compounds [MAK Value Documentation, 2006]". In: *The MAK-Collection for Occupational Health and Safety*. Wiley-VCH Verlag GmbH and Co. KGaA, pp. 282–307.

[42] N.N. Greenwood and A. Earnshow. *Chemistry of the Elements*. 2nd ed. Elsevier, 1997. ISBN: 978-0-7506-3365-9.

[43] V. Lenher. "The non-existence of tellurium oxychloride." In: *Journal of the American Chemical Society* 31.2 (1909), pp. 243–244.

[44] B. A. van Brussel and J. Th. M. De Hosson. "Glancing angle x-ray diffraction: A different approach". In: *Applied Physics Letters* 64.12 (1994), pp. 1585–1587.

[45] W.E. Swartz. "X-ray photoelectron spectroscopy". In: *Analytical Chemistry* 45.9 (1973), 788A–800a.

[46] M. K. Bahl, R. L. Watson, and K. J. Irgolic. "X-ray photoemission studies of tellurium and some of its compounds". In: *The Journal of Chemical Physics* 66.12 (1977), pp. 5526–5535.

[47] C. B. Itkin V. P.and Alcock. "The O-Te (oxygen-tellurium) system". In: *Journal of Phase Equilibria* 17.6 (1996), pp. 533–538. ISSN: 1054-9714.

A Appendix

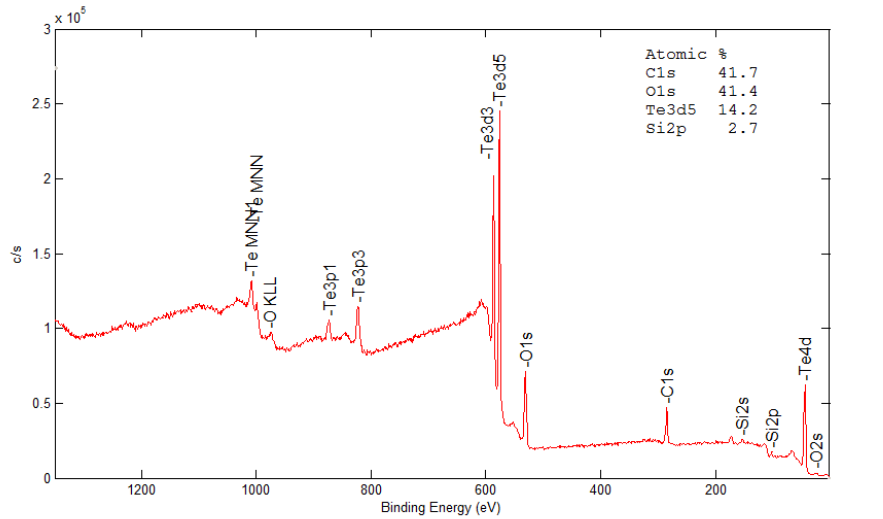

Figure 20. The whole X-ray photoelectron spectroscopy spectrum, from the deposition made on the zinc under oxidizing conditions.

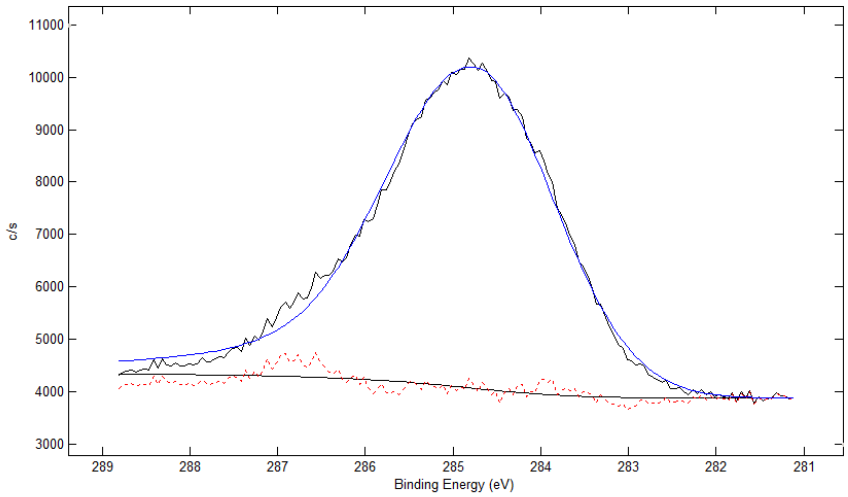

Figure 21. The focused X-ray photoelectron spectroscopy spectrum, from the deposition made on the zinc under oxidizing conditions, showing the peak belonging to carbon, C1s.

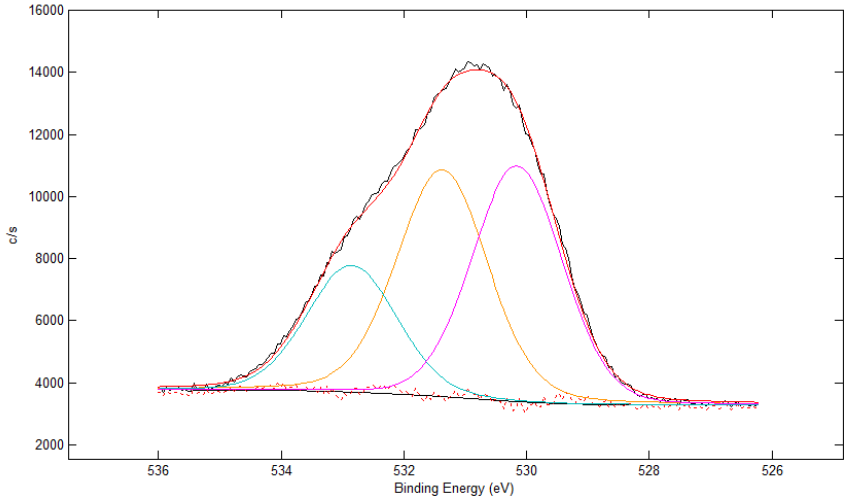

Figure 22. The focused X-ray photoelectron spectroscopy spectrum, from the deposition made on the zinc under oxidizing conditions, showing the peak belonging to oxygen, O1s.

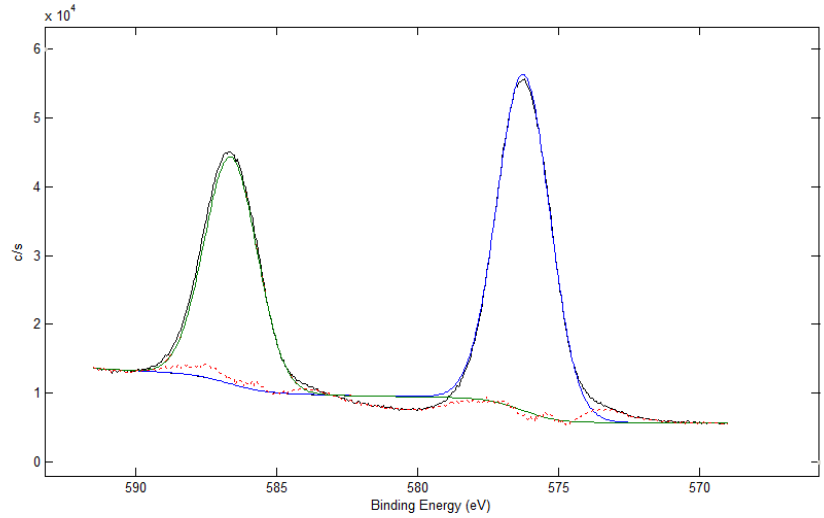

Figure 23. The focused X-ray photoelectron spectroscopy spectrum, from the deposition made on the zinc under oxidizing conditions, showing the peaks belonging to tellurium, Te3d3 and Te3d5.